Helsinki University of Technology Radio Laboratory Publications

Teknillisen korkeakoulun Radiolaboratorion julkaisuja

Espoo, February, 2002 REPORT S 251

EXPERIMENTAL ANALYSIS OF MULTIDIMENSIONAL RADIO CHANNELS

Thesis for the degree of Doctor of Science in Technology

Kimmo Kalliola

TEKNILLINEN KORKEAKOULU
TEKNISKA HÖGSKOLAN
HELSINKI UNIVERSITY OF TECHNOLOGY
TECHNISCHE UNIVERSITÄT HELSINKI
UNIVERSITE DE TECHNOLOGIE D'HELSINKI

Helsinki University of Technology Radio Laboratory Publications
Teknillisen korkeakoulun Radiolaboratorion julkaisuja
Espoo, February, 2002 REPORT S 251

EXPERIMENTAL ANALYSIS OF MULTIDIMENSIONAL RADIO CHANNELS

Kimmo Kalliola

Dissertation for the degree of Doctor of Science in Technology to be presented with due permission for public examination and debate in Auditorium S4 at Helsinki University of Technology (Espoo, Finland) on the 15th of February 2002 at 12 o'clock noon.

Helsinki University of Technology
Department of Electrical and Communications Engineering
Radio Laboratory

Teknillinen korkeakoulu
Sähkö- ja tietoliikennetekniikan osasto
Radiolaboratorio

PREFACE

This thesis work has been done at the Radio Laboratory of the Institute of Digital Communications (until 2000 Institute of Radio Communications), Helsinki University of Technology, during years 1997-2001. The work has been done under several projects, funded by the National Technology Agency of Finland (TEKES) and Finnish telecommunications companies. The work has also been partly funded by the Graduate School in Electronics, Telecommunications, and Automation (GETA). I thank Radio Laboratory and GETA for the possibility to carry out the work. In addition, I am grateful to the Foundation of Technology, the Finnish Society of Electronics Engineers, Nokia Foundation, HPY Foundation, and Wihuri Foundation for the financial support I have received during the work.

I am grateful to my supervisor Professor Pertti Vainikainen for his numerous ideas and encouragement, without which this work would not have been completed. I also warmly thank Prof. Mark Beach and Dr. Robert Bultitude for reviewing this thesis and for their valuable suggestions.

All my co-workers and friends at the Radio Laboratory, Nokia Research Center, Vienna University of Technology, and VTT deserve thanks for their company and assistance. From the Radio Laboratory I want to mention especially Pauli Aikio, Jarmo Kivinen, Martti Toikka, and Lasse Vuokko, whose contributions to the experimental work were significant. Also Eino Kahra, Lauri Laakso, and Lorenz Schmuckli deserve special acknowledgment for the mechanical realizations of the measurement equipment.

My friends and co-authors of the joint publications Heikki Laitinen, Juha Laurila, and Kati Sulonen I want to thank for their significant contribution in the publications. I also thank Professor Ernst Bonek, as well as Klaus Hugl and Martin Toeltsch from his group in the Institute of Communications and Radio-Frequency Engineering in Vienna University of Technology for the fruitful cooperation. I also wish to thank my friend Matti Leppänen for his help in electronics design, as well as Outi Kivekäs, Joonas Krogerus, and Veli Voipio for their contribution to the antenna element design and measurements.

I want to thank my fellow students Jani Ollikainen and Lauri Sumanen for keeping up the academic peer pressure, which has contributed to realizing this thesis. My parents I wish to thank for their support in the course of my studies. Finally, I would like to thank my wife Satu for her love and patience during my often irregular working hours.

Helsinki, January 13, 2002

Kimmo Kalliola

ABSTRACT

In this thesis new systems for radio channel measurements including space and polarization dimensions are developed for studying the radio propagation in wideband mobile communication systems. Multidimensional channel characterization is required for building channel models for new systems capable of exploiting the spatial nature of the channel. It also gives insight into the dominant propagation mechanisms in complex radio environments, where their prediction is difficult, such as urban and indoor environments.

The measurement systems are based on the HUT/IDC wideband radio channel sounder, which was extended to enable real-time multiple output channel measurements at practical mobile speeds at frequencies up to 18 GHz. Two dual-polarized antenna arrays were constructed for 2 GHz, having suitable properties for characterizing the 3-D spatial radio channel at both ends of a mobile communication link. These implementations and their performance analysis are presented.

The usefulness of the developed measurement systems is demonstrated by performing channel measurements at 2 GHz and analyzing the experimental data. Spatial channels of both the mobile and base stations are analyzed, as well as the double-directional channel that fully characterizes the propagation between two antennas. It is shown through sample results that spatial domain channel measurements can be used to gain knowledge on the dominant propagation mechanisms or verify the current assumptions. Also new statistical information about scatterer distribution at the mobile station in urban environment is presented based on extensive real-time measurements. The developed techniques and collected experimental data form a good basis for further comparison with existing deterministic propagation models and development of new spatial channel models.

CONTENTS

LIST OF PUBLICATIONS

[P1] K. Kalliola and P. Vainikainen, "Characterization system for radio channel of adaptive array antennas," *Proceedings of 8th IEEE International Symposium on Personal, Indoor and Mobile Radio Communications (PIMRC'97),* Helsinki, Finland, September 1-4, 1997, pp. 95-99.

[P2] K. Kalliola, H. Laitinen, L. I. Vaskelainen, and P. Vainikainen, "Real-time 3D spatial-temporal dual-polarized measurement of wideband radio channel at mobile station," *IEEE Transactions on Instrumentation and Measurement*, vol. 49, no. 2, pp. 439-448, April 2000.

[P3] J. Laurila, K. Kalliola, M. Toeltsch, K. Hugl, P. Vainikainen, and E. Bonek, "Wide-band 3-D characterization of mobile radio channels in urban environment," *Accepted for publication in IEEE Transactions on Antennas and Propagation.*

[P4] M. Toeltsch, J. Laurila, K. Kalliola, A. F. Molisch, P. Vainikainen, and E. Bonek, "Statistical characterization of urban spatial radio channels," *Accepted for publication in IEEE Journal on Selected Areas on Communications*.

[P5] K. Kalliola, H. Laitinen, K. Sulonen, L. Vuokko, and P. Vainikainen, "Directional radio channel measurements at mobile station in different radio environments at 2.15 GHz," *Proceedings of 4th European Personal Mobile Communications Conference (EPMCC2001)*, Vienna, Austria, February 20-22, 2001, CD-ROM ÖVE 27 (ISBN 3-85133-023-4), pap113.pdf.

[P6] K. Kalliola, K. Sulonen, H. Laitinen, O. Kivekäs, J. Krogerus, and P. Vainikainen, "Angular power distribution and mean effective gain of mobile antenna in different propagation environments," *Accepted for publication in IEEE Transactions on Vehicular Technology*.

In papers [P1], [P5], and [P6], this author had the main responsibility for preparing the papers and conducting the measurements and analysis presented in the papers, supervised by Pertti Vainikainen. The experimental work for papers [P5] and [P6] was planned and performed in collaboration with this author and Heikki Laitinen. Lasse Vuokko assisted in data processing for [P5]. In [P6], Kati Sulonen and Joonas Krogerus measured and Outi Kivekäs simulated the radiation patterns of the evaluated antennas. Kati Sulonen also performed the mean effective gain computations. In [P2], this author prepared the paper and was responsible for the design and implementation of the spherical antenna array, making the test measurements, and conducting the performance analysis of the measurement concept. The direction-of-arrival estimation methods were developed in co-operation with this author and Heikki Laitinen, who implemented the numeric beam synthesis calculations based on algorithms by Leo Vaskelainen. Pertti Vainikainen supervised the work. In papers [P3] and [P4] this author was responsible for implementing the measurement system while the authors planned and performed the measurements together. Juha Laurila and Martin Toeltsch were mainly responsible for the data analysis and preparing the papers. The interpretation of the results was done in co-operation by all authors. Pertti Vainikainen and Ernst Bonek supervised the work.

1. INTRODUCTION

The increasing information flow is the main driver of the development of wireless communication systems today. Until recently the mobile radio networks have been circuit-switched and originally designed for voice transmission. The current second generation (2G) digital systems support also data transmission at low bit rates (~10 kbits/s). The most widely used of these systems is the worldwide GSM (Global System for Mobile Communications) [1]. In the course of writing this thesis, the third generation (3G) systems, often referred to as UMTS [2] are being taken into use. Unlike 2G, the 3G systems are optimized for transmission of packet data at high bit rates (up to 2Mbits/s). They enable transmission of high quality images and video, and provide access to the internet from mobile terminals. Even higher bit rates for limited coverage areas can be achieved with wireless local area networks (WLANs), up to 54 Mbits/s for example in ETSI HIPERLAN standard [3].

The key difference between data transmission using wireline and through radio channel is that in the latter case the transmission media is common for all users in a certain geographical area. Achieving high throughput data rates requires optimized use of the limited radio resources. Considerable effort is today focused in radio propagation research and developing methods for increasing the spectral efficiency of future wireless systems, e.g. within the European COST framework [4,5]. Common to these methods is that they aim to optimize the radio interface, which is the matching element between the wireline and the wireless radio channel. Since the radio propagation channel is a complex function of time, frequency, and space, an adaptive interface is required for optimal performance.

Instead of suffering from the nonideal effects of mobile radio channel (multipath fading, delay and angle distortion, polarization cross coupling), the radio interfaces of the upcoming new systems will be capable of tolerating and even benefiting from these effects. The radio systems will exploit the spatial dimension of the radio channel to reduce interference and gain capacity by introducing smart antennas at the base and/or mobile stations [6-8]. Term smart antenna refers to a configuration of multiple antenna elements, the signals of which are weighted in an intelligent manner so that the signal-to-interference-and-noise ratio (SINR) of the combined signal is maximized by applying beamforming [9] or diversity techniques [10]. The SINR gain can be turned into increased capacity or coverage of the radio network.

The optimization of smart antenna algorithms [11,12], requires realistic radio channel simulation models including the spatial dimension [13-15]. Also channels recorded with antenna arrays can be used in simulations, provided that they are appropriately selected [14]. The cellular network planning for smart antennas [16] in different environments and performance evaluation of smart antenna network configurations requires reliable models for predicting the radio propagation. Due to the complexity of urban and indoor propagation environments, spatial channel measurements [4,17] are needed for verification of the models. Stochastic models [15] require experimental data to tune them, while deterministic models need measurements to verify the assumptions of the physical propagation mechanisms [19,20].

In addition to improving the network capacity or coverage, the spatial information of the radio channel at the base station, i.e. the direction-of-arrival (DoA) and propagation delay of the re-

ceived radio signal, can be utilized in cellular network-based positioning methods [21-23] used in the emerging mobile location services. Furthermore, performance evaluation of mobile terminal antennas requires reliable models of the angular distribution of incident power at the mobile station in various propagation environments [24,25]. Especially it is essential to understand the effect of the radio channel on the polarization of the transmitted electrical field in the case of handheld radios.

So far most of the reported directional radio channel measurements have been limited to measuring only the azimuth angle dimension at the base station, e.g. [26-28]. This is adequate in most cases from the point of view of developing spatial processing algorithms for smart antenna base stations. However, for analyzing the propagation mechanisms in urban and indoor environment and their modeling it is necessary to take also the elevation angles of the multipaths into consideration. It is evident that at the mobile station the radio environment is three-dimensional [29-31], and full 3-D measurements are required for characterizing it properly. Such measurements for static channels have been reported previously in [29,30,32,33]. However, real-time measurements are required for capturing the time-variant channel behavior, such as line-of-sight (LOS) – non-line-of-sight (NLOS) transients, and collecting large amounts of data for angular power distributions at the mobile station.

1.1 OBJECTIVES OF THE WORK

The aim of this thesis work is to develop new systems for radio channel measurements including space and polarization dimensions for studying the radio propagation in wideband mobile communication systems. The delay dimension has been left for less consideration, since it has been studied widely previously. The temporal and directional resolution of the measurements are as high as feasible in order to make the results independent of any particular radio transmission system. In addition, measurement techniques are developed for both ends of the channel, i.e. the fixed and mobile stations, which usually have different type of local surroundings and thus experience different directional channel properties.

The work also aims to give general insight of spatial radio channel properties and propagation mechanisms in urban environments at 2 GHz frequency range, through analysis of experimental data. The purpose is to provide a basis for evaluation of existing deterministic propagation models and for development of spatial channel models.

1.2 CONTENTS OF THE THESIS

In this thesis work, the radio channel sounder of Helsinki University of Technology (HUT), Institute of Digital Communications (IDC), was extended to enable the measurement of channel impulse responses from multiple receiving antenna elements. The system was first presented and its limitations analyzed in [P1]. For extracting the DoA information of the incident waves at the receiver, antenna arrays and beamforming techniques were developed. The use of a spherical antenna array for studying the 3-D radio environment of a mobile station is described in [P2]. Paper [P3] describes the features of the directional radio channel at an urban base station showing clusterization of the incident waves. In paper [P4], the experimental data presented in [P3] is examined in more detail, through statistical analysis of the channel from the perspective of a beamforming base station antenna. Paper [P5] describes the directional distribution of incident power and cross polarization power ratio at the mobile station in dif-

ferent radio environments. In [P6], two parameterized models are fitted to the experimental elevation power distributions presented in [P5], and the distributions are applied for analysis of mean effective gain of practical mobile handset antennas.

2. MOBILE RADIO CHANNEL

2.1 INTRODUCTION

The propagation path from a radio transmitter antenna to a receiver antenna is called the *radio propagation channel*. In telecommunications the definition of *radio channel* often covers the full radio interface with antennas. However, in this work the terms radio channel and radio propagation channel will be used interchangeably to denote the physical channel between a pair of antennas.

In a wireless system, the transmitted wave interacts with the physical environment in complex ways, and arrives at the receiver along a number of paths, referred to as multipaths. The ratio of transmitted and received field strengths, i.e. the propagation loss, is determined by the distance due to the square-law spreading and ground reflections, as well as absorption by materials and foliage in the propagation path. Multipath propagation results in the spreading of power in delay (or time) and angle (or space) dimensions. Movement of the transmitter, receiver, or any other object in the physical channel causes spreading also in Doppler (or frequency) dimension [6] and makes the channel time-variant. Furthermore, the polarization of the transmitted electromagnetic field changes before it reaches the receiver. The efficient employment of spatial processing in modern wireless communication systems requires thorough knowledge of the mobile radio channel in the operating environment.

2.2 PROPAGATION MECHANISMS

The interactions of waves with various objects in the environment, such as the ground, buildings, vegetation, lamp posts, etc. are commonly referred to as propagation mechanisms, e.g. [14]. The dominant propagation mechanisms are briefly described in the following.

2.2.1 Free space path loss

The power radiated by a transmitter antenna spreads to all directions in space and thus only part of it can be collected by the receiver antenna. The free space path loss, i.e. the ratio of the transmitted and received power depends on the gain of the transmitter antenna (in the direction of the receiver antenna), the distance between the antennas, and the effective aperture of the receiver antenna. The path loss is usually written using the receiver antenna gain instead of the effective aperture:

$$L_p = \frac{P_t}{P_r} = \left[G_t \frac{1}{4\pi r^2} A_{eff,r} \right]^{-1} = \left[G_t G_r \left(\frac{\lambda}{4\pi r} \right)^2 \right]^{-1} \tag{2.1}$$

In (2.1) $A_{eff,r}$ is the effective aperture of the receiver antenna, G_r and G_t are the receiver and transmitter antenna gains, λ is the wavelength, and r is the distance between the antennas. The equation is valid if the antennas are in free space. In practice it is sufficient that the first Fresnel zone is free from obstructions. At 2 GHz the maximum diameter of the first Fresnel zone is 3 meters, when the distance from the transmitter is 30 m.

2.2.2 Reflection and refraction

2.2.2.1 Specular reflection

When a plane wave propagating in one medium encounters a flat, infinite boundary with another medium with different electromagnetic properties, it will be partially reflected back into the first medium, and partially transmitted (refracted) into the second medium. The basic property of specular reflection is that the direction of the reflected wave is symmetric to the direction of the incident wave with respect to the surface normal. The magnitudes of the reflected and refracted waves can be computed from the well-known Fresnel's formulas, e.g. [34]. The reflection and refraction coefficients are different for polarizations parallel and perpendicular to the plane containing the normal of the boundary and the propagation direction,which can lead to a change of wave polarization. Infinite surfaces do not exist in reality, and in practice it is sufficient that the surface is larger than the cross-section of the first Fresnel zone [34].

2.2.2.2 Diffuse reflection

A rough surface presents many facets to the incident wave, and the reflection mechanism is more like scattering (see 2.2.4), whose properties are unpredictable due to the random nature of the surface. The contribution of diffuse properties depends on both the surface roughness and the incidence angle. The Rayleigh criterion for the surface roughness is written as [34]:

$$C = \frac{4\pi\sigma\cos\alpha}{\lambda} \tag{2.2}$$

where σ is the standard deviation of the surface irregularities, α is the angle of incidence with respect to the normal of the surface, and λ is the wavelength. The surface is smooth and specular reflection dominates if $C < 0.1$. For $C > 10$ the reflection is highly diffuse, and the specularly reflected wave is small enough to be neglected. At frequencies close to 2 GHz ($\lambda \approx 15$ cm), specular reflection dominates if the surface roughness is less than 1 mm or 7 cm for normal and near-grazing ($\alpha = 89°$) incidence, respectively. For highly diffuse reflection the corresponding values are 10 cm and 7 m. It can be concluded that in the frequency range around 2 GHz the reflections from the ground or from (outer) building walls are neither purely specular nor completely diffuse.

2.2.3 Diffraction

Since only finite surfaces exist in reality, also edges and corners need to be considered. Diffraction can be analyzed based on Huygens' principle stating that each element of a wavefront at any time can be considered as the center of a new spherical wave and that the position of the wavefront at any later time is the envelope of all such spherical waves. The field strength in the shadow region behind an ideally conducting half-screen (knife-edge) can be computed from Kirchoff's approximation, e.g. [35]. Complex diffraction coefficients for separate rays can be derived from the Uniform geometrical theory of diffraction (UTD) [36]. Heuristic equations for UTD diffraction coefficients for wedges of lossy dielectric materials, such as those typically used in buildings, are given in [37,38]. In contrast to the reflection, a single ray

incident upon a wedge at an angle α to the edge produces a cone of diffracted rays so that the semi-angle of the cone is equal to α.

2.2.4 Scattering

Scattering is a general interaction process between electromagnetic waves and various objects. Regularly shaped objects that are large compared to the wavelength can be treated with the approximations introduced above. Instead, small and irregularly shaped objects, such as trees, lampposts, or irregularities in building walls (see 2.2.2.2), are considered as scatterers. Scattering causes energy to be reradiated in many different directions.

2.3 PROPAGATION MODELS

The design, optimization, and performance evaluation of radio communication systems requires simulations with models featuring the relevant characteristics of the radio propagation in the operating environment. Propagation models can be classified as deterministic and stochastic [15]. Deterministic models are based on exact computations making use of information of the specific physical environment. Stochastic models aim to describe on average the propagation phenomena, and the model parameters need to be tuned to feature the characteristics of the given environment. The tuning is usually based on measurements, but also accurate deterministic models can be used for the purpose. In addition to models, link-level system simulations can also be made using stored channel responses, e.g. [39]. This approach requires storing large amounts of data to obtain a representative dataset containing the characteristic behavior of the environment.

2.3.1 Deterministic models

2.3.1.1 Simplified pathloss models

Several models have traditionally been used for prediction of path-loss in macrocell environments. These models are empirical (i.e. based on measurements) and take into account some physical properties of the environment. Probably the most well-known path loss model is the Okumura–Hata model, which is based on measurements by Okumura in and around Tokyo city and was later approximated by a set of formulae by Hata [40]. The model is valid in the frequency range from 150 MHz to 1000 MHz and takes into account the environment type (large city, medium-small city, suburban, open), the base and mobile antenna heights, and frequency. In the European COST (Cooperation in Science and Technology) 231 project [18] the model was extended to cover also frequencies between 1500 MHz and 2000 MHz in urban/suburban environments [18].

The Walfisch–Bertoni model [41] allows slightly more detailed characterization of the environment by taking into account the average building height and spacing as well as the width and relative orientation of the roads. In this model diffractions over all rooftops except the last one before the mobile are treated as knife-edge diffractions. In COST231 project [18], the Walfisch-Bertoni model was combined with Ikegami's model [42] for the diffraction from the last building down to the street canyon. In addition, empirical correction factors were intro-

duced to improve agreement with measurements. An error was later found in these factors, and corrected in [43].

2.3.1.2 Site-specific models

Site-specific propagation models aim at predicting the properties of the propagation mechanisms presented in Section 2.2., using techniques issuing from solving Maxwell's equations [19]. They rely on the availability of a detailed database of the geometry of the physical environment in the region under study. If the antenna heights are low compared to the building height, it is adequate to model only the two-dimensional database of the building footprints. In a more general case it is necessary to have a database of buildings in three dimensions. Naturally also indoor modeling relies on the availability of a 3-D database. In addition to the geometry, also the electromagnetic parameters of the materials need to be included in the database.

Site-specific models for outdoor applications are based on ray optical methods: GTD or UTD [19,44]. For indoor modeling also the more precise finite-difference time domain (FDTD) method has been proposed [45]. The most commonly used ray method is ray tracing, in which rays are launched from the transmitter into several directions covering the full 4π solid angle, and traced until they reach the receiver or fall below a threshold field strength [46].

Site-specific propagation models have proven useful in coverage predictions in cell planning, especially in street microcell environments where propagation over rooftops is negligible [15,44]. However, the greatest potential of these models is in that they can produce an accurate representation of the wideband impulse response of the radio channel including the direction-of-arrival (DoA) at both ends of the channel. This property makes them attractive for cell planning for smart antenna systems. Still measurements including the DoA are required to verify the realism of existing ray tracing models.

2.3.2 Stochastic models

In simplest form, for narrowband applications, stochastic propagation models need to include only the received power and fading distribution due to complex summation of multipath amplitudes. For wideband applications also the time dispersion of the channel has to be included. Furthermore, with the introduction of techniques depending on the spatial channel properties, also spatial information needs to be modeled [13].

Several models have been developed that include the time dispersion of the wideband channel, by describing it as a sum of weighted and delayed Dirac responses. Examples of this type of models are the COST207 model [47] and its successors CODIT [48] and ATDMA [49] models. The weights are stochastic processes with parameters fitted to measurement data in different types of environments. A stochastic channel model including also the incidence direction of each path and designed for broadband indoor applications is presented in [50].

Classical model by Clarke [51] gives an analytic solution for the Doppler distribution of the narrowband channel. It is based on a very simple assumption of the geometrical distribution of scatterer distribution around the mobile station. To extend stochastic channel models to in-

clude also the directions of arrival of the multipaths, more accurate models for the scatterer distribution in the vicinity of both the mobile and base station antennas are required. A stochastic geometry-based spatial channel model is presented in [52]. In the recent years, the European COST action 259 (successor to COST207 and COST231) has developed a set of geometry-based channel models that include the DoAs at the base station and at the mobile station [4]. These *double-directional* models provide a complete description of the radio channel in all dimensions and they are expected to become widely used. However, there is still a need for directional radio channel measurements to verify the models and to select appropriate parameters for different types of radio environments. An overview of different measurement concepts and performed measurement campaigns is presented in [17]. In the ultimate case the deterministic models would be accurate enough to allow parameter extraction for stochastic models.

3. MULTIDIMENSIONAL CHANNEL MEASUREMENTS

3.1 INTRODUCTION

Traditionally path loss measurements have been used in comparison with deterministic propagation models for evaluating their accuracy, e.g. [41,46]. In simplified path loss models this approach may lead to good results, but the drawback is that it may support also erroneous assumptions about propagation phenomena. Multidimensional radio channel measurements including the angle and delay dimensions are required for reliable characterization of the propagation. Also stochastic spatial channel models require directional data for extraction of correct parameter values.

From a system point of view the radio channel can be characterized using a transfer function including all possible dimensions. Figure 1 illustrates the radio propagation channel between a pair of antennas.

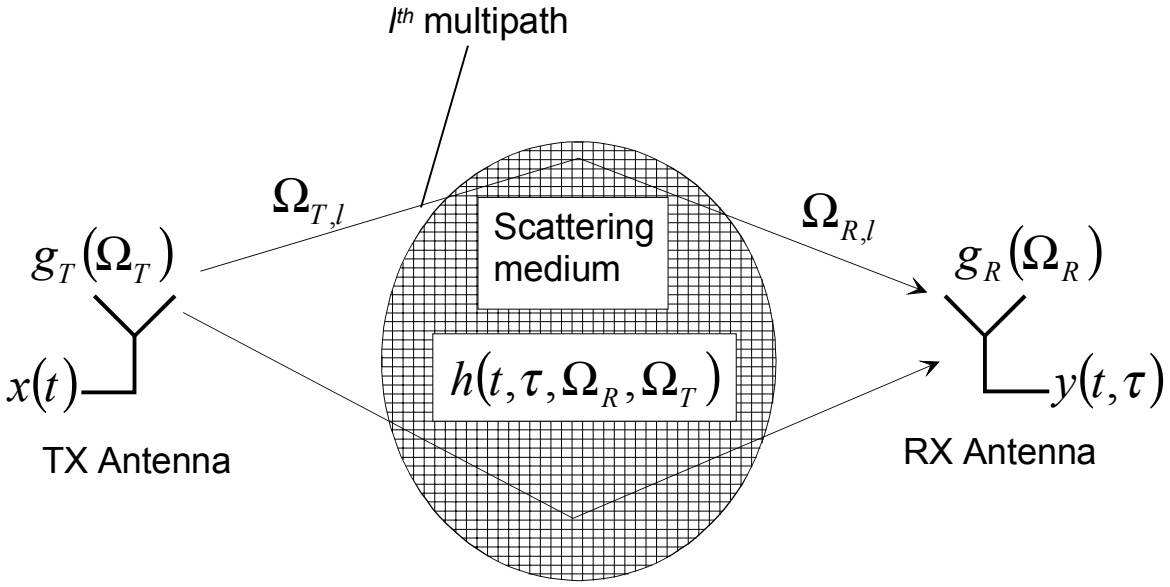

Figure 1. Radio propagation channel between a pair of antennas.

Time-variant signal *x(t)* is transmitted by the TX antenna. Part of the transmitted energy reaches the RX antenna after propagating through different paths. Thus the signal at the output of the RX antenna consists of a sum of multiple attenuated, phase-shifted, and time-delayed replicas of signal *x(t)* and is given by:

$$y(t,\tau)=\sum_{n=1}^{L(t)}\left[\alpha_l(t)\delta(\tau-\tau_l(t))\cdot x(t)\right]=h(t,\tau)\otimes x(t) \tag{3.1}$$

In (3.1) $L(t)$ denotes the number of multipaths at a given time instant, and $\alpha_l(t)$ and $\tau_l(t)$ are the complex amplitude and propagation delay corresponding to l^{th} multipath, respectively. $h(t,\tau)$ is called the time-variant *channel impulse response* (CIR) and $\otimes$ denotes convolution. The CIR can be decomposed to the integral of the directional angle resolved CIR (DCIR) at the RX antenna weighted by the complex radiation pattern of the antenna over all *directions of arrival* Ω_R [1]:

$$h(t,\tau)=\int_{\Omega_R}\left[h^V(t,\tau,\Omega_R)g_R^V(\Omega_R)+h^H(t,\tau,\Omega_R)g_R^H(\Omega_R)\right]d\Omega_R \tag{3.2}$$

Superscripts V and H denote the vertically and horizontally polarized components of the directional channel impulse response and complex radiation pattern. Direction of arrival Ω_R is determined in 3-D coordinates, and specified by azimuth angle ϕ and elevation angle θ. Equation (3.2) can be written in matrix form as:

$$h(t,\tau)=\int_{\Omega_R}\mathbf{h}^{\mathrm{T}}(t,\tau,\Omega_R)\mathbf{g}_R(\Omega_R)d\Omega_R \tag{3.3}$$

where:

$$\mathbf{h}(t,\tau,\Omega_R)=\begin{bmatrix}h^V(t,\tau,\Omega_R)\\ h^H(t,\tau,\Omega_R)\end{bmatrix},\qquad \mathbf{g}_R(\Omega_R)=\begin{bmatrix}g^V(\Omega_R)\\ g^H(\Omega_R)\end{bmatrix} \tag{3.4}$$

The vertically and horizontally polarized components of the DCIR at the RX antenna can be further decomposed to the integrals of the *double-directional* angle resolved channel impulse response (DDCIR) weighted by the complex radiation pattern of the TX antenna over all *directions of departure*:

$$\begin{aligned}h^V(t,\tau,\Omega_R)&=\int_{\Omega_T}\left[h^{VV}(t,\tau,\Omega_R,\Omega_T)g_T^V(\Omega_T)+h^{HV}(t,\tau,\Omega_R,\Omega_T)g_T^H(\Omega_T)\right]d\Omega_T\\ h^H(t,\tau,\Omega_R)&=\int_{\Omega_T}\left[h^{VH}(t,\tau,\Omega_R,\Omega_T)g_T^V(\Omega_T)+h^{HH}(t,\tau,\Omega_R,\Omega_T)g_T^H(\Omega_T)\right]d\Omega_T\end{aligned} \tag{3.5}$$

Equation (3.5) can be written in matrix form as:

$$\mathbf{h}(t,\tau,\Omega_R)=\int_{\Omega_T}\mathbf{h}^{\mathrm{T}}(t,\tau,\Omega_R,\Omega_T)\mathbf{g}_T(\Omega_T)d\Omega_T \tag{3.6}$$

where:

$$\mathbf{h}(t,\tau,\Omega_R,\Omega_T)=\begin{bmatrix}h^{VV}(t,\tau,\Omega_R,\Omega_T) & h^{VH}(t,\tau,\Omega_R,\Omega_T)\\ h^{HV}(t,\tau,\Omega_R,\Omega_T) & h^{HH}(t,\tau,\Omega_R,\Omega_T)\end{bmatrix} \tag{3.7}$$

[1] the formulas are presented for polarization-independent case in [4]

The matrix defined in (3.7) is called polarization coupling matrix [53], and it describes the co- and cross-coupling of vertically (VP) and horizontally (HP) polarized fields in the radio channel, as illustrated in Figure 2.

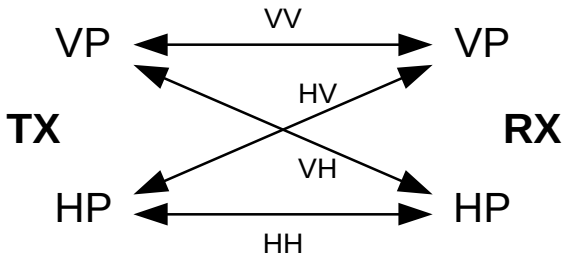

Figure 2. Schematic plot of polarization coupling between a pair of antennas.

The multidimensional radio channel between a pair of antennas (see Fig. 1) and corresponding to a certain carrier frequency is completely described by the polarization-dependent double-directional angle resolved impulse response defined in Eq. (3.7). Each term of the matrix in (3.7) can be written as a sum of the multipath components as:

$$h(t,\tau,\Omega_R,\Omega_T)=\sum_{l=1}^{L(t)}\alpha_l(t)\delta(\tau-\tau_l(t))\delta(\Omega_R-\Omega_{R,l}(t))\delta(\Omega_T-\Omega_{T,l}(t)) \tag{3.8}$$

where $\Omega_{R,l}(t)$ and $\Omega_{T,l}(t)$ are the direction of arrival (DoA) and direction of departure (DoD) of l^{th} multipath, respectively. δ denotes Dirac's delta function.

The DDCIR can be measured by scanning through all directions of departure with a narrow-beam antenna transmitting a known signal, and measuring the following parameters of all signal multipath components arriving at the RX antenna:

- complex amplitude
- Doppler shift
- propagation delay
- direction of arrival
- polarization state

Since the channel is a function of carrier frequency, the measurement needs to be made at the desired frequency range. Also, the investigation of instantaneous correlation of uplink and downlink channels in a frequency-division-duplex (FDD) system requires simultaneous (or almost simultaneous, see 3.4.3.2) measurement at two frequencies. Resolving all terms of the polarization coupling matrix requires separate transmission at two orthogonal polarizations. In practice, scanning through all directions of departure at the transmitter end is infeasible. In a time-invariant case the DoDs can be found by interchanging the TX and RX and repeating the measurement. It must be taken into account that the obtained result is weighted by the radiation pattern of the transmitter antenna. The real-time measurement of the time-variant double-directional radio channel requires using antenna arrays at both ends of the link (see 3.4.5).

3.2 MEASUREMENT OF COMPLEX AMPLITUDE AND DOPPLER SHIFT

The measurement of amplitude and phase of the incident wavefront requires coherent reception at the transmit frequency. Coherent means that the local oscillator of the receiver must be synchronized to that of the transmitter. In practice the synchronization can be achieved by using stable primary frequency standards for both oscillators. The phase difference of a single delay tap in successive impulse responses gives the Doppler shift of the corresponding multipath. The measurement of Doppler shift requires real-time measurement, i.e. the measurement rate has to be at least twice the maximum Doppler shift of the channel, according to Nyquist criterion.

3.3 MEASUREMENT OF PROPAGATION DELAY

The measurement of the propagation delay of the multipaths requires the use of a synchronized reference channel with an exactly known delay, i.e. a cable connection between the transmitter and receiver. In practice this is only feasible at relatively short measurement distances. However, when the local oscillators of the transmitter and receiver are locked to stable frequency standards, the propagation delay can be solved from the excess delay based on a LOS reference measurement at a known distance. The excess delay of a multipath stands for the time difference between the first received channel component and the multipath. The excess delay is obtained by measuring the wideband impulse response $h(\tau,t)$ of the radio channel [54,55]. Wideband measurement techniques can be divided into pulse and continuous-waveform techniques [56]. Continuous-waveform techniques can be further divided to frequency sweeping (or hopping) and direct-sequence techniques [56]. In frequency-domain sounding techniques the impulse response is obtained from the measured frequency transfer function $H(f,t)$ of the channel through inverse Fourier transform. In a time-domain measurement the basic requirement is that the repetition period of the transmitted signal is longer than the maximum excess delay, to obtain an unambiguous result. Typically the achieved delay resolution depends directly on the measurement bandwidth, but some more sophisticated methods exist for achieving better resolution [57,58]. The ultimate lower limit for the uncertainty of the delay measurement depends in addition to the bandwidth also on the signal-to-noise ratio of the signal, and is given by the Cramér-Rao lower bound [59].

3.4 MEASUREMENT OF DOA

3.4.1 Requirements

The need for DoA measurements stems from the directional dispersion of the radio channel. The properties of the dispersion depend strongly on the local scattering environment around the antenna. For example the scattering environments at the base and mobile stations are typically different. At a high-elevated base station the scatterers are concentrated close to the horizontal plane. Therefore it is often adequate to measure only the azimuth angle of the incident waves, and typically also in a limited azimuth sector. On the other hand, in urban and indoor environments the scattering environment around the mobile station is three-dimensional [29,30,31], leading to a need for omnidirectional measurement in azimuth and over a wide elevation angle range. The DoA measurement is based on using an antenna configuration capable of directional scanning, either mechanical or electronic. The measurement techniques

can be divided into two classes depending on the requirements they set to the time variance of the channel.

3.4.2 Stationary methods

The static DoA measurement methods are based on using a single receiver antenna. These methods are based on mechanic scanning and they do not capture the Doppler dimension of the channel.

3.4.2.1 Rotation of narrow-beam antenna

The straightforward method for DoA measurement is to mechanically rotate a narrow-beam high-gain receiving antenna. The basic requirement is that the directional channel properties do not change during one full rotation of the antenna. This method has been used for characterizing the azimuth power profile at the base station [60-62], for indoor propagation measurements [63], and for measuring the 3-D power distribution at the mobile station [24,64,65].

3.4.2.2 Synthetic aperture method

Another method that has been used for DoA measurements with a single antenna is the synthetic aperture technique [66]. Also this method is limited to time-invariant channels, since it is based on mechanical spatial scanning, i.e. moving a single sensor between different locations and measuring one impulse response in each location. Another possibility is to move the sensor at constant speed and measure one impulse response at fixed time intervals. The DoA information is extracted from the relative phases of the signal multipath components received at different spatial locations by using techniques described in Sec. 3.4.4. The synthetic aperture method is sensitive to frequency differences between the local oscillators of transmitter and receiver. Frequency difference leads to phase drift, which transforms into angular offset in space domain. The geometry of the spatial grid determines the directional properties of the measurement: 3-D measurement requires 2-D grid. The synthetic aperture technique has been used for spatial measurements at the base station [26,27], and at the mobile station in [29,30,32,33,67].

3.4.3 Real-time methods

The real-time measurement methods capture also the Doppler dimension of the channel. These methods are based on using multiple antenna elements and electronic directional scanning.

3.4.3.1 Multichannel receiver

The only true real-time method for spatio-temporal measurement of a time-variant radio channel is to coherently receive signals from an antenna array with a multichannel vector sounder. As in the synthetic aperture approach, the DoA information is extracted from the relative phases of the elements. Furthermore, the measured channels can be recorded and used directly as part of a smart antenna system simulator. The multichannel receiver approach is, however, very complex and expensive, since one calibrated receiver branch must exist for each antenna

element. Measurement equipment using this kind of technique has been developed at least within the ACTS project TSUNAMI II [68], in the GloMo Effort of Virginia Tech [69], and in McMaster University, Canada [70].

3.4.3.2 RF-switching

A technique for making real-time spatial radio channel measurements using a single receiver and an antenna array was first presented in [P1], and practically at the same time in [71]. In this technique the receiver is connected to one of the array elements at a time using a fast RF switch (multiplexer). The switching can be made so fast that all three dimensions (delay, Doppler, spatial) of the radio channel can be measured at practical mobile speeds [P1]. The technique has been used also e.g. in [72-74]. The fast measurement also facilitates the acquisition of large amounts of data for statistical distributions, and thus enables the parameter extraction for stochastic channel models, which would otherwise be very time-consuming.

In addition to the DoA information, the real-time multichannel measurement systems enable the investigation of different diversity reception approaches. Diversity reception relies on the availability of two or more independent replicas of the same information signal. The evaluation of various RX and TX diversity configurations - space, polarization, pattern diversity, or a combination of those - requires reception (and transmission) with several signal branches. In the case of a switched multichannel measurement system the switching rate must be such that the channels among all RX and TX antennas are sampled before there are any significat changes on the channels so that the recorded data contain the same attributes as they would have if sampled simultaneously. The diversity gain can be estimated based on the correlation properties of the signals received from the diversity branches [75]. The RF-switching method also offers a practical way to study the correlation properties of uplink and downlink channels in an FDD system.

3.4.4 Electronic DoA estimation techniques

The extraction of the directional information from synthetic aperture or antenna array measurements is based either on conventional beamforming (Fourier processing), e.g. [P1], or some more sophisticated algorithms that offer greater angular resolution. Such algorithms are e.g. the Space-Alternating Generalized Expectation-Maximization (SAGE) algorithm [76], applied for channel measurements in [73,76,77], and the Unitary ESPRIT algorithm, developed by Zoltowski et al [78], and applied e.g. in [26,29,74]. The SAGE algorithm is based on maximum-likelihood estimation, and is independent of the array geometry. Instead, ESPRIT is a subspace algorithm and as such limited to uniform linear or planar array geometries, but it has lately been modified to handle also circular array geometries [79]. In addition, an extension of the algorithm has been developed recently [80], which enables the joint estimation of all measured channel dimensions in double-directional measurements. The DoA measurement techniques involving antenna arrays require phase calibration of the receiver branches. The relative phases of the branches are measured using an injected calibration signal or with a network analyzer, and the data are corrected at the post-processing phase. Also potentially different phases of radiation patterns of individual array elements need to be compensated.

3.4.5 Double-directional and MIMO measurements

A straightforward way of resolving the DoDs of the channel multipaths is to combine the DoA information measured at both ends of the channel, as is presented in Sec. 5.1.2 of this thesis. Based on reciprocity of the radio channel it is also possible to apply the DoA measurement methods described in the previous sections for measuring the DoD. The double-directional angle resolved impulse response is obtained by applying directional scanning techniques at both ends of the channel. Measurements combining synthetic aperture at the transmitter and RF switching at the receiver have been reported in [80,81]

Real-time measurement of the double-directional angle resolved impulse response requires a Multiple-Input Multiple-Output (MIMO) measurement system with multiple channels and antenna arrays at both TX and RX ends of the channel, e.g. [82,83]. Also the analysis of actual MIMO systems [7] that rely on the availability of independent propagation paths between two multielement antennas requires a similar measurement setup. Examples of MIMO measurements can be found e.g. in [84-86]. The transmission channels need to be separated in code or time domains by employing orthogonal codes [84] or antenna switching [85,86]. At the receiver either a switched array [85] or a multichannel sounder [84,86] has to be used.

Double-directional radio channel measurement allows reliable tracking of propagation paths with up to three multiple reflections/diffractions. The last scattering objects before the wave reaches the base and mobile stations can be identified precisely, which enables the investigations of different physical propagation mechanisms in urban environments. This information is highly valuable when evaluating and further developing site-specific deterministic propagation models.

3.5 MEASUREMENT OF POLARIZATION STATE

The measurement of the polarization state of the incident wavefront requires two measurements at the same physical location, with two orthogonal receiver antenna polarizations, and identical beam patterns for both polarizations. In static channel conditions this can be done by changing the orientation of a single antenna with suitable beam properties. However, a real-time measurement of the polarization of a time-variant radio channel requires simultaneous reception at both polarizations, or alternatively RF multiplexing between two separate feeds of a dual-polarized antenna. The measurement of the full polarization coupling matrix requires separate transmission at two orthogonal polarizations. In real-time this can only be done with the MIMO measurement techniques presented in the previous section.

4. DEVELOPED MEASUREMENT TECHNIQUES

4.1 MULTICHANNEL MEASUREMENT SYSTEM

The multidimensional radio channel measurements presented in this thesis are all based on RF multiplexing of an antenna array. The used measurement system is based on the wideband complex radio channel sounder developed at Helsinki University of Technology / Institute of Digital Communications. The sounder is described in detail in [87]. For spatial measurements, the receiver is equipped with a fast RF switching unit working up to 18 GHz to periodically acquire channel impulse responses from multiple receiving sensors (elements of antenna array). The system was presented for the first time in [P1].

4.1.1 Principle

The timing diagram of the multichannel measurement is presented in Figure 3. The measurement is burst-wise: the sampling period is T_s, while the measurement period is T_m. T_c is the code period, which is equal to the delay window (maximum unambiguously solved excess delay). The channel period T_{ch} must be chosen as an integer number of code periods in order to retain the delay synchronism in successive measured impulse responses.

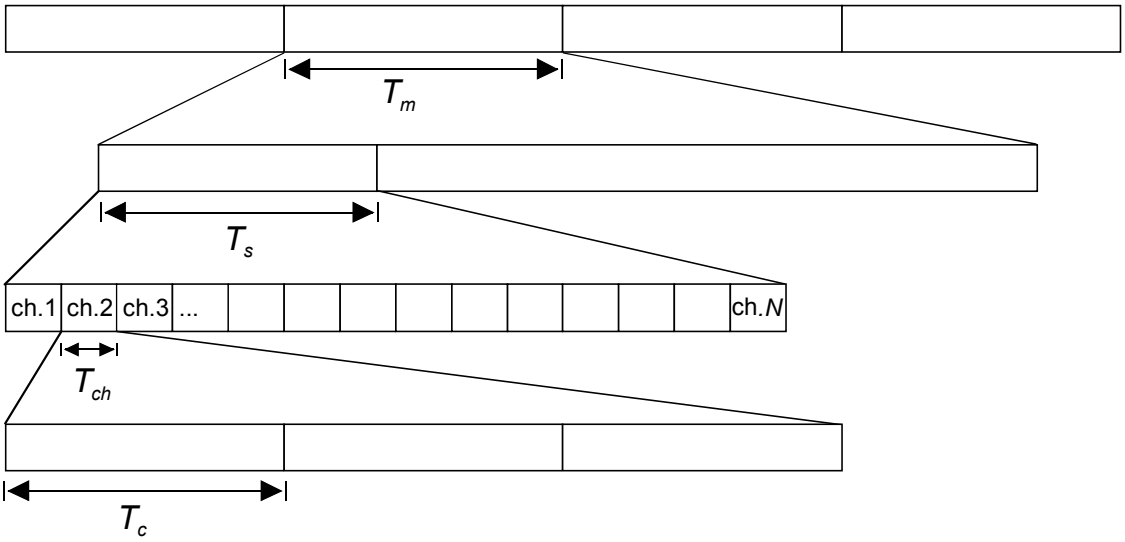

Figure 3. Timing diagram of multichannel measurement.

During the sampling period, the RF switch scans through all N input channels. The system was recently upgraded for *MIMO* measurements by adding an RF switch also to the transmitter [83]. This multiplies the sampling period by the number of output channels.

4.1.2 Limitations

Real-time multichannel measurement produces large amounts of data. In [P1], the bottleneck of the IDC sounder was the storage capacity, which was limited to 8 MB of on-board memory of the sampling boards. When the memory was full, the measurement had to be stopped for transferring the data to the hard disk of a PC via an ISA bus. This made the multichannel measurement very slow and the continuously measured path length infeasibly short, only of the order of a few meters with 64 input channels. To expand the capacity, an external sampling and storage unit, capable of storing data at a rate of R=2×15 Ms/s (I+Q) directly to two SCSI hard disks was specified in this work and purchased in 2000.

Table 1 presents the performance limits of the multichannel measurement for a typical setup, and formulas for their calculation. The values are computed for sampling frequency (f_s) of 120 MHz, chip frequency (f_c) of 30 MHz, code length (L_c) of 127 chips (4.23 µs delay window). The spatial sampling period is one fifth of a wavelength, and the signal is sampled with 8 bits. In theory, the burst size (P), which is proportional to the number of measured channels, is limited by the 4 MB of on-board memory buffer of the external sampling boards. However, the data burst is temporarily stored on the PC's random access memory (RAM) before it is written to the hard disk, and in practice the operating system limits the maximum continuous RAM block and thus the burst size to 1 MB. The maximum route length is limited by the size of the 9 GB hard disks (C).

Table 1. Performance limits of multichannel measurement system.

Max. number of channels	$N_{\max} = \dfrac{P}{L_c \cdot \dfrac{f_s}{f_c}} = \dfrac{1\,\text{MB}}{127\,\text{bytes} \cdot \dfrac{120\,\text{MHz}}{30\,\text{MHz}}} = 2064$
Max. measurement rate with 64 channels	$f_{m,\max} = \dfrac{R}{N \cdot L_c \cdot \dfrac{f_s}{f_c}} = \dfrac{15\,\text{MB/s}}{64 \cdot 127\,\text{bytes} \cdot \dfrac{120\,\text{MHz}}{30\,\text{MHz}}} \approx 460\,\text{Hz}$
Max. continuous route length with 64 channels	$s_{\max} = \dfrac{C}{N \cdot L_c \cdot \dfrac{f_s}{f_c}} \cdot \dfrac{\lambda}{5} = \dfrac{9\,\text{Gbytes}}{64 \cdot 127\,\text{bytes} \cdot \dfrac{120\,\text{MHz}}{30\,\text{MHz}}} \cdot \dfrac{\lambda}{5} \approx 55000\,\lambda$

To capture the Doppler dimension of the channel, the measurement rate has to be at least twice the maximum Doppler shift of the channel. Thus the maximum mobile speed corresponding to the maximum measurement rate of 460 Hz is 34 m/s at 2 GHz, or 3.8 m/s at 18 GHz carrier frequency. Correspondingly the maximum continuous measurement route lengths with 64 channels for 2 and 18 GHz are 8.3 km and 920 m. These values are clearly high enough to enable continuous real-time multidimensional channel measurements at practical mobile speeds over routes that are long enough to represent the characteristic propagation behavior in the environment.

In array measurements with the switching method the Doppler effect causes also phase rotation between subsequent array elements. Provided that the time-variance of the channel is caused solely by the mobile's one movement, the phase rotation due to the movement can be solved based on the phase rotation of a single element [88]. If not compensated, the phase rotation transforms into offset in angular domain. For example, if the maximum allowed DoA error for Fourier beamforming and a uniform linear array with $\lambda/2$ element spacing is p % of the 3 dB beamwidth at broadside, the maximum number of array elements can be written as a function of the maximum Doppler shift and the channel period as [88]

$$N \leq \frac{p}{100} \cdot \frac{0.886}{f_{D,\max} \cdot T_{ch}} \tag{4.1}$$

In (4.1) it is assumed that the elements are scanned consecutively from one end to the other. Figure 4 presents the maximum number of elements as the function of maximum Doppler shift and delay window (assuming that $T_{ch} = T_c$) for a maximum offset of 10 % of the 3 dB broadside beamwidth.

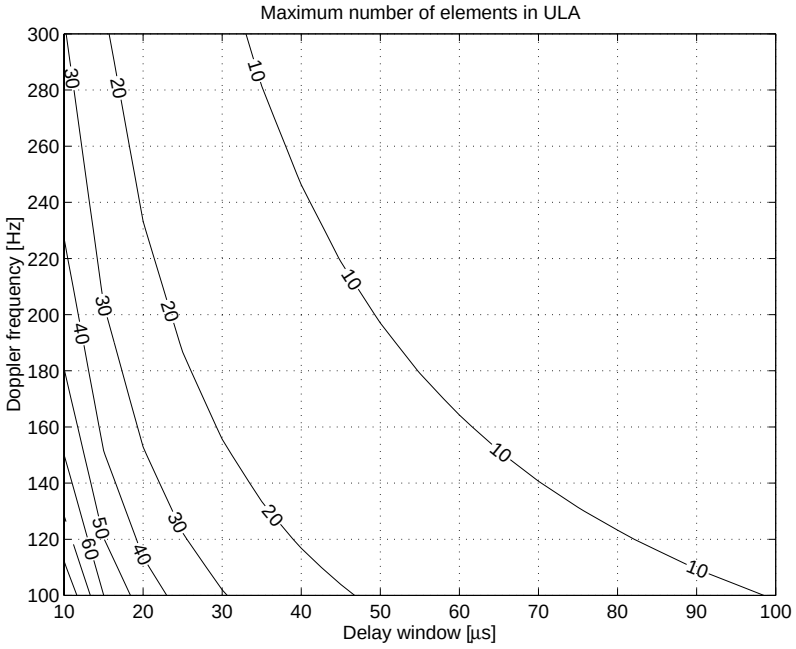

Figure 4. Maximum number of elements in uniform linear array with half-wavelength element spacing for a maximum offset of 10 % of 3 dB broadside beamwidth for Fourier beamforming.

It can be seen in Figure 4 that in practice the Doppler effect limits the element number only at rather large delay windows. For example, a maximum excess delay of 20 µs corresponds to a propagation path that is 6 km longer than the shortest path between the transmitter and receiver. Such propagation delays usually exist only in mountainous areas and most often the Doppler effect does not limit the number of channels or mobile speed in channel measurements based on the switched array technique. With other than linear array geometries the phase errors due to Doppler effect are smaller, and element scanning order can be used to

minimize the effect on measured DoA. The DoA error caused by the Doppler effect in the case of beamforming with a spherical array was analyzed in [P2]. For other DoA estimation methods than Fourier processing, such as ESPRIT and SAGE, the relation between the DoA accuracy and Doppler shift is not that straightforward.

4.1.3 Constructed switching units

The requirements for the RF switching unit include low insertion loss (since the switch is the first component after the antenna), high isolation to reduce mutual coupling, and a fast switching rate to ensure channel stationarity inside the time period of scanning through the input channels. During this thesis work two switching units have been designed for the IDC multichannel measurement system.

The RF switching unit presented in [88,P1] has only 8 input channels, and it was designed for the 2 GHz frequency band. To obtain reasonable angular resolution in 3-D spatial radio channel measurements with two orthogonal polarizations, a switching unit with 64 input channels was designed. In addition, a 32-channel switching unit operating in the frequency range of 1…18 GHz was constructed to enable multichannel measurements also above 2 GHz. Two different switch technologies were used: fast GaAs FET switches for the 2 GHz band, and PIN-diode switches with low insertion loss for higher frequencies. The former enables subchip switching (t_{sw} = 3 ns) while the latter has a longer settling time (t_{sw} = 200 ns), and a guard time is required to avoid spurious peaks in the data. Normally a guard time of one code period is used to retain delay synchronism in successive measured impulse responses. The insertion loss of the GaAs FET switch is 9.5 dB at 2 GHz, and the minimum isolation only 20 dB. The performance of the PIN-diode switch is much better; it has a 3.3 dB insertion loss at 5 GHz (~5 dB at 18 GHz), and a minimum isolation of approximately 70 dB.

4.2 HIGH-RESOLUTION 3-D MEASUREMENT AT BASE STATION

4.2.1 Requirements

The efficient use of smart base station (BS) antennas in urban environments requires thorough knowledge of the spatial channel dimension. The propagation mechanisms in urban environments need to be understood in order to develop channel models for evaluating different smart antenna concepts. Spatial channel measurements at the BS have been reported in several papers, e.g. in [26,28,73]. Both dynamic and static measurements have been conducted, but they have been limited to describe only the azimuth angle dimension of the channel. In a macrocell base station, where the antenna is located above the average rooftop level, the surroundings is typically open, and the distances to the scatterers vary from tens to thousands of meters. In such conditions the identification of dominant propagation mechanisms (e.g. over-rooftop diffraction, reflections from high-rising buildings) requires high resolution in azimuth, elevation, and delay. In addition, the investigation of the polarization properties of different propagation mechanisms requires a dual-polarized measurement. During this thesis work, a high-resolution 3-D measurement method was applied to investigate the dominant propagation mechanisms in an urban macrocell (downtown Helsinki) [P3]. The method combines RF switching and synthetic aperture techniques.

4.2.2 Construction of planar synthetic aperture

The synthetic aperture was formed using a physical array of 16 dual-polarized microstrip patch elements installed above each other on a trolley with vertical and horizontal orientation of polarization axes. The elements were arranged in a zigzag pattern and their spacing was 0.5λ in both directions. This structure reduces the mutual coupling between the elements because the smallest interelement distance is between the corners of the patches. The measured magnitude of the mutual coupling between the co-polarized terminals of two diagonally neighboring elements was –27 dB. The 3 dB beamwidth of the elements is 70º for both polarizations. The trolley that was equipped with an electrical motor moved at a constant speed of 0.3 m/s over metallic rails to collect "snapshots" over the physical array at certain horizontal positions. During the measurement, one impulse response was collected from all dual-polarized elements of the physical array at each 0.5λ distance moved by the trolley, and thus a planar grid with $0.5\lambda \times 0.5\lambda$ spacing was formed. The size of the planar synthetic aperture was 8×29 wavelengths, which is adequate to obtain high angular resolution (approximately 6° in elevation and 2° in azimuth by conventional beamforming).

4.2.3 Limitations

The basic requirement of the synthetic aperture measurement is that the channel does not change during the whole data collection period. Therefore, the measurements were performed during night with minimum traffic. The snapshots in the different horizontal positions of the array were taken with intervals of 0.2 s, which lead to a total data collection period of 14.5 s. According to the analysis presented in [P3], the repeatability of the measurement was found good in the absence of traffic in the vicinity of the mobile antenna. Another potential error sources are the uncertainty of the trolley velocity and the frequency difference of the synthesizers at the transmitter and receiver. The phase measurement in LOS link with known DoA was used to check the velocity and to tune the Rubidium clocks of the sounder. The constant movement of the trolley was negligible, since the snapshot collection period was only 544 μs, corresponding to array movement of only 163 μm (0.001λ).

4.2.4 DoA estimation method and accuracy

After reorganizing the data to correspond a planar structure, the DoAs corresponding to each local maxima in the power delay profile were computed by using 2-D Unitary ESPRIT [78], a subspace-based super-resolution algorithm. The algorithm was implemented at the Institute of Communications and Radio-Frequency Engineering (INTHF) of Vienna University of Technology (TUWien). See [P3] for details. After estimating the azimuth and elevation angles of the incoming waves at each active delay sample, narrow pencil beams where formed in these directions and the powers carried by the waves both in horizontal and vertical polarization were detected.

LOS measurements with exactly known transmitter positions were used to validate the accuracy of the measurement concept. The estimated LOS DoAs corresponded to the real values within an estimation error of less than 1º. This error is mainly caused by practical inaccuracies of the measurement configuration (such as wind load on the physical array or rail misalignment). The error is so small that the reliable tracking of last scatterers before the antenna was possible [P3].

4.3 ISOTROPIC 3-D MEASUREMENT AT MOBILE STATION

4.3.1 Requirements

In contrast to the base station, the scattering environment around the mobile station (MS) in urban and indoor environment is three-dimensional [29-31]. Thus the investigation of dominant propagation mechanisms requires DoA measurement covering the entire 4π solid angle. In addition, the time-variant channel behavior (e.g. transients) cannot be characterized with static measurements. Real-time measurement of the 3-D radio channel requires fast reception from elements of an antenna array with a geometry that allows the separation of incident waves in both azimuth and elevation.

In addition, the evaluation of mobile handset antennas in realistic operating environments requires knowledge of the angular distribution of the incident θ- and ϕ-polarized power at the antenna [P6]. The angular power distributions at the mobile station can be determined by performing extensive measurement campaigns in realistic environments. Previously, the synthetic aperture measurement approach has been applied for such measurements [29,30,33,89]. Also directional scanning with a narrow-beam antenna has been used [24,64,65]. Both methods are, however, very slow, and thus infeasible for collecting large amounts of data for angular power distributions.

During this thesis work a real-time method for 3-D channel measurements at the mobile station was developed. The method is based on using a spherical array configuration of dual-polarized elements, and it is the only reported method allowing the complete real-time spatio-temporal characterization of the wideband 3-D mobile radio channel.

4.3.2 Spherical antenna array[2]

To enable directional scanning over the entire 4π solid angle, a spherical antenna array was constructed. The geometry of the built array is based on the dual of the Archimedian solid, the truncated icosahedron, which is probably best known today as the geometry of the soccer ball [90]. The array has 32 dual-polarized elements, with an inter-element distance of $0.641R$ or $0.714R$ (R is the radius of the sphere). Every element has either five or six neighbors. The elements are mounted on a surface consisting of two hollow aluminum hemispheres. The elements are pointed towards the normal of the sphere and oriented so that the polarization vectors corresponding to the feeds (ϕ and θ) are parallel to unit vectors $\mathbf{u}_\phi$ and $\mathbf{u}_\theta$, respectively. Figure 5 presents a photograph of the spherical array. The 64-channel RF switching unit is placed inside the sphere together with its control electronics.

[2] The traditional concept of an antenna array is defined as a system of identical and identically oriented antennas with similar current distributions. The configuration presented here does not fit into this definition. However, for consistency, it is called a spherical array in this thesis.

Figure 5. Spherical array for 3-D radio channel measurement at mobile station.

4.3.3 DoA estimation

The analysis presented in this thesis is based on DoA estimation using beamforming [P2]. The delay taps were first identified by detecting the local maxima of the power delay profile (PDP) averaged over the array elements. Only such maxima were detected, whose power exceeded a threshold level, computed by finding a silent interval in the PDP, and adding 2 dB to the maximum value in the silent interval. However, the threshold was never below −27 dB relative to the maximum of the PDP. Corresponding to each delay tap, there may exist one multipath component or several components separated by their DoAs (and also delays within the resolution of the channel sounder). Up to four multipath components per delay tap were estimated using the beamforming scheme with pre-computed array weights (2° beam spacing in azimuth and elevation), as described in [P2]. Only such multipaths were accepted whose amplitude exceeded a threshold value of 6 dB below the highest multipath, in order to filter out spurious signals due to sidelobes of the array. The measured sidelobe level of the array is approximately −10 dB in the case of two simultaneous multipaths [P2], but the level increases with an increasing number of multipaths.

Also numeric beam synthesis was tested for the DoA estimation [91]. It can produce slightly more optimized patterns in some cases, but is computationally more complex. The SAGE al-

gorithm [14] was recently implemented in HUT/IDC, to improve the angular resolution of the measurement [92]. All results presented in this thesis were obtained using the beamforming method.

4.3.4 Performance analysis

The directional properties of the measurement system were analyzed in [P2] by measuring a known radio channel in an anechoic chamber. The main drawback of the spherical array is the poor angular resolution and limited angular dynamic range (in [P2] called spatial dynamic range), determined by the sidelobes of the spherical array. However, when the temporal resolution of the measurement is high, the problem is significantly alleviated. The total spatial resolution of the measurement is determined by the angular resolution of the spherical array of approximately 40° and the delay resolution of the channel sounder. For example, by measuring with the HUT channel sounder at a chip frequency of 30 MHz, the spatially separable blocks are truncated cones with an opening angle of 40° and length of 10 m, and the size of the block increases with increasing distance between the last scattering point and the array. More closely spaced waves sum up at the receiver in a complex manner, which causes uncertainty in the estimated DoA. The number of individual waves inside a resolved multipath, or actually a *multipath group* can be analyzed based on its fast fading distribution.

Figure 6 shows the cumulative fast fading distribution of the resolved multipath groups in spherical array measurements in urban environment. To compensate for the effect of large scale fading the powers of the resolved multipath groups were normalized to the local mean power (averaged over a distance of approximately 30 wavelengths) at each point. Also a fitted Ricean distribution with Rice factor K=11.9 dB is presented, and for comparison also the Rayleigh distribution. The measured distribution was obtained from a large number of urban outdoor measurement routes (over two million resolved multipath groups in roughly 300 000 angle resolved impulse responses). It can be seen in Figure 6 that the measured distribution agrees well with the Ricean distribution except of probability levels below 10 %. At all probability levels the distribution is clearly closer to the Ricean distribution than the Rayleigh distribution. The result indicates that the resolved multipath groups on average contain a dominant component that is approximately 12 dB stronger than the diffuse components. In indoor measurements the fitted Rice factor was K=9.5 dB. According to the analysis the resolved multipaths can be considered with fair accuracy to be composed of one dominant wave in both urban and indoor environments.

The return loss of the array elements measured in place in the array was higher than 10 dB over the 100 MHz bandwidth of the sounder receiver. Thus it can be concluded that the distortion of the signal due to impedance mismatch is very small and could not be observed in calibration measurements performed in an anechoic chamber.

When measuring the polarization properties of the incident waves, the cross-polarization discrimination (XPD) of the measurement antenna affects the obtained result. For example, assuming a measurement antenna with a constant XPD of 17 dB, a true XPR of 11 dB would be underestimated by approximately 1 dB in the measurement. The measured mean XPD of the spherical array is 17 dB and the XPD has a ±4 dB peak-to-peak ripple as a function of incidence angle [P2].

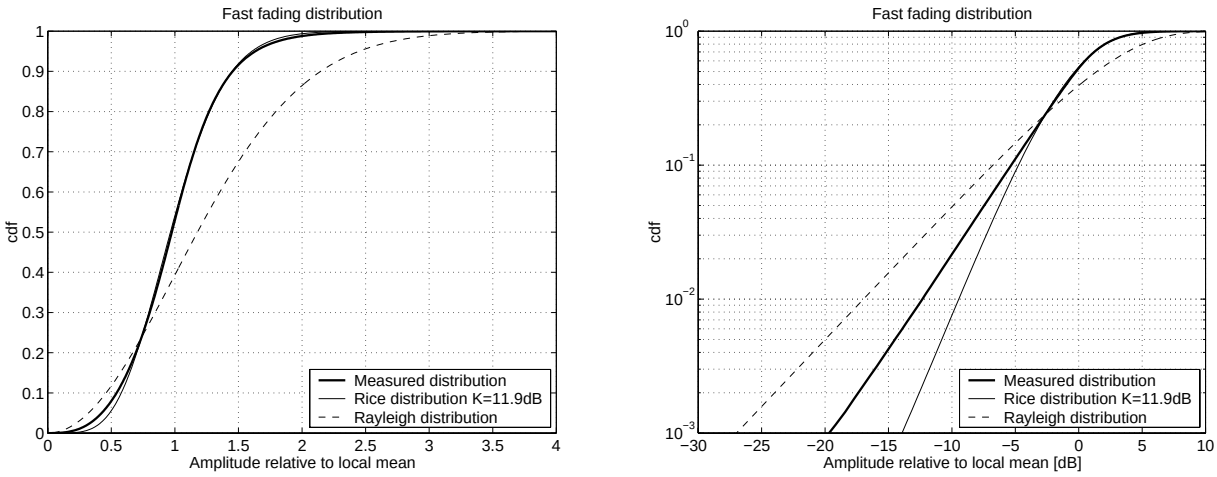

Linear scale *Logarithmic scale*

Figure 6. Fast fading distribution of resolved multipath groups. Average over all urban outdoor measurement routes.

5. ANALYSIS OF EXPERIMENTAL DATA

This chapter demonstrates how spatial domain channel measurements can be used to gain knowledge about radio propagation in urban environment. Sample results of measurements performed using the techniques described in the previous chapter are presented and analyzed.

5.1 IDENTIFICATION OF PROPAGATION MECHANISMS

Comparing the measured DoAs and delays of the multipath signal components to the geometry enables the identification of the last scattering objects before the wave reaches the antenna. Double-directional measurement, i.e. measuring the channel at both ends of the link enables the identification of individual propagation paths or propagation clusters. This is illustrated by the following two examples.

5.1.1 Continuous directional measurement at mobile station [P5]

Figure 7 shows a measurement route in an urban environment characterized by a regular grid of street canyons. The BS antenna was mounted 8 m above street level, while the average building height in the area is approximately 25 m. Figures 8 and 9 present the distribution of incident power at the mobile station vs. azimuth and elevation angles along the route, measured using the measurement method based on a spherical array, described in Sec. 4.3. Figure 10 presents the power vs. propagation delay along the route. The spherical array was at height of 1.7 m above street level. The variation of the received power has been removed from the results by normalizing to the total received power at each point of the route.

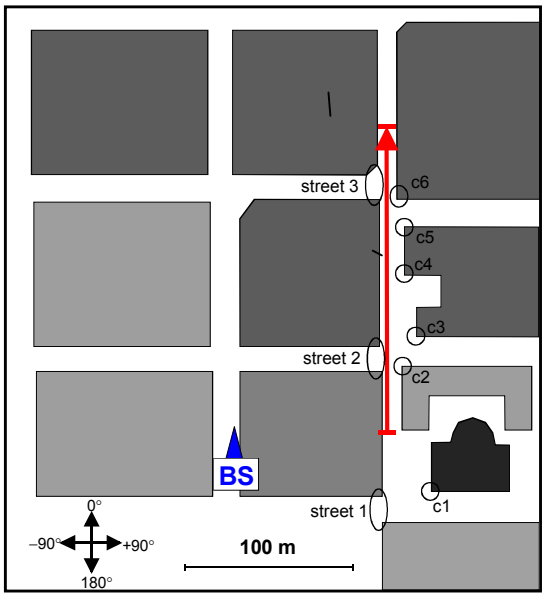

Figure 7. Microcell measurement route.

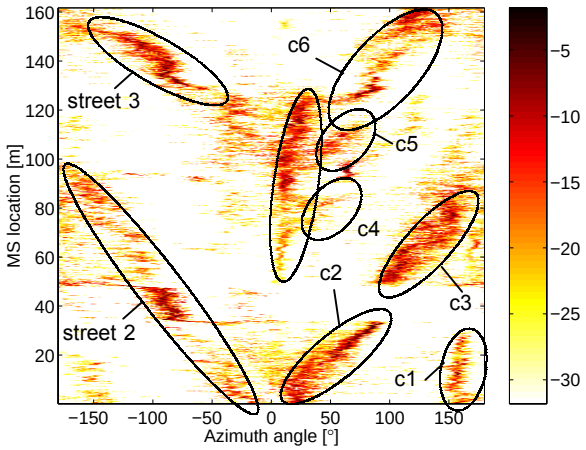

Figure 8. Azimuth power distribution at the mobile station along the route.

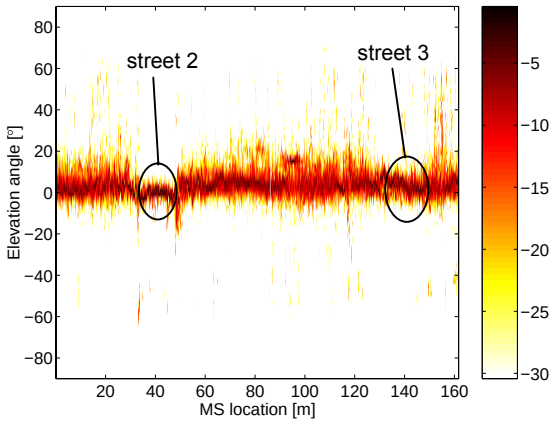

Figure 9. Elevation power distribution along the route.

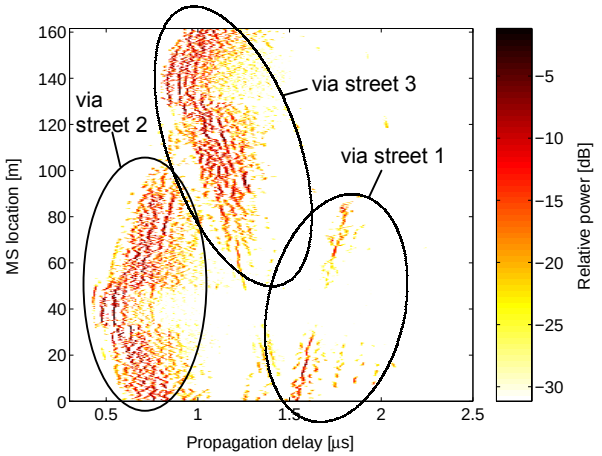

Figure 10. Power vs. propagation delay along the route.

Figure 8 reveals that the power is concentrated around a few dominant secondary sources. In addition, plenty of diffuse signal components exist from the local scattering environment around the mobile. The azimuth angles of the dominant sources correspond well to the angles of the two side streets ('street 2', 'street 3', see Fig. 7), as well as the angles of the building block corners ('c1...c6'). It can be noticed in Fig. 8 that the strongest secondary sources are the block corners on the opposite side of the street than the base station, except for when the mobile is bypassing the side streets. For the rest of the route the diffractions from the side street corners at left are clearly weaker than those from the corners at right. The result agrees with previous measurements by Bergljung et al, who showed in [93] that the major contributor to the diffracted field in the side street is the opposite corner of the street junction. Figure 9 shows that most power is received from angles smaller than 20° above the horizontal plane. This indicates that no waves propagate over building rooftops, but the propagation takes place in street canyons. The mean elevation angle decreases when bypassing the two side streets. The street-canyon-guided propagation is demonstrated in Fig. 10, where three delay clusters can be found, corresponding to waves propagated via the three side streets. According to the results shown above and in [P5], it is apparent that if the base station antenna is mounted clearly below the rooftop level the radio propagation between the BS and MS in urban environment mainly occurs via street canyons by reflecting from building walls and ground and diffracting from building block corners.

5.1.2 Double-directional measurement in urban macrocell

The following measurement example is based on double-directional channel measurements, performed separately at the base and mobile stations by interchanging the transmitter and receiver. Figure 11 presents a map of the measurement area. The mobile station was located in a street canyon, at a distance of approximately 450 m from the base station. The BS antenna height was 27 m, which is slightly above the average rooftop level of the area. The measurement was performed using the spherical array (Sec.4.3) at the mobile station and the synthetic aperture technique (Sec. 4.2) at the base station. Figure 12 shows the measured power-delay profile, averaged over the elements of the spherical array. The azimuth-delay-power profiles measured at the mobile and base stations are shown in Figs. 13 and 14, respectively. Similarly, Figs. 15…18 present the power over elevation-delay and azimuth-elevation planes.

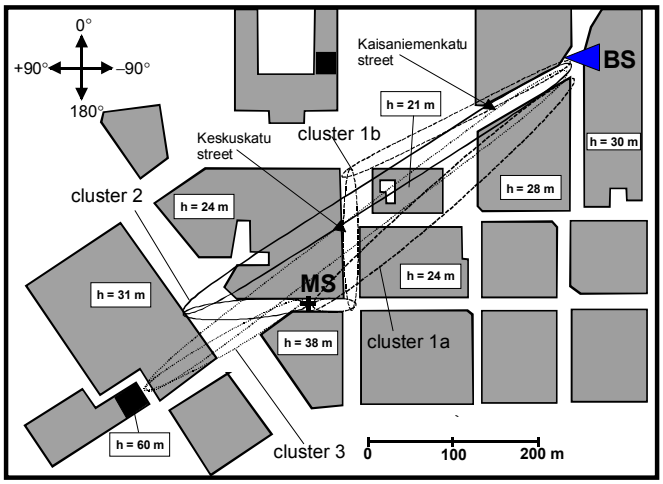

Figure 11. Propagation clusters on map.

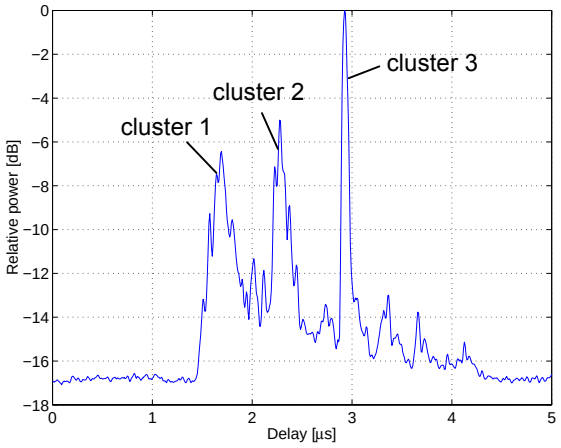

Figure 12. Average power-delay profile.

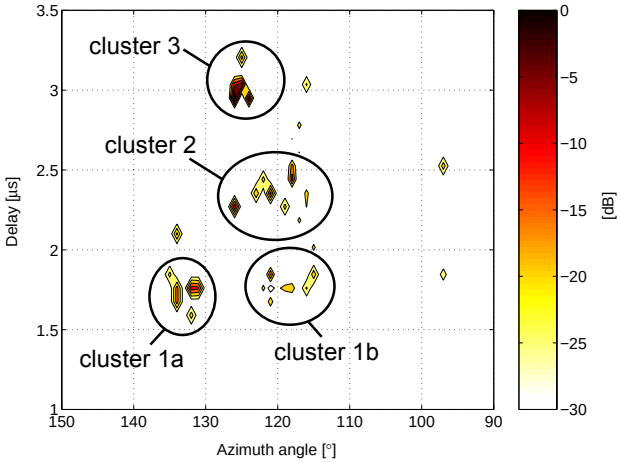

Figure 13. Azimuth-delay-power profile at *base station*.

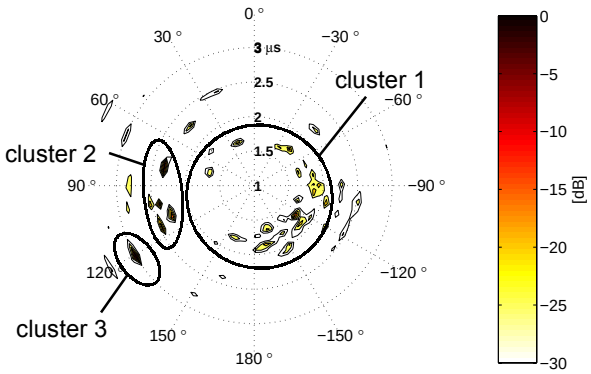

Figure 14. Azimuth-delay-power profile at *mobile station*

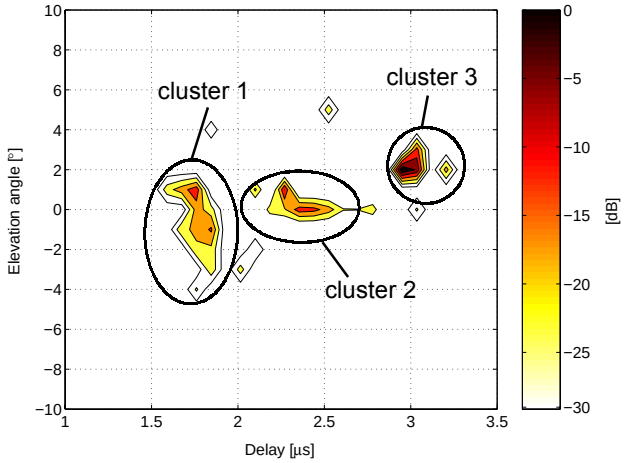

Figure 15. Elevation-delay-power profile at *base station*.

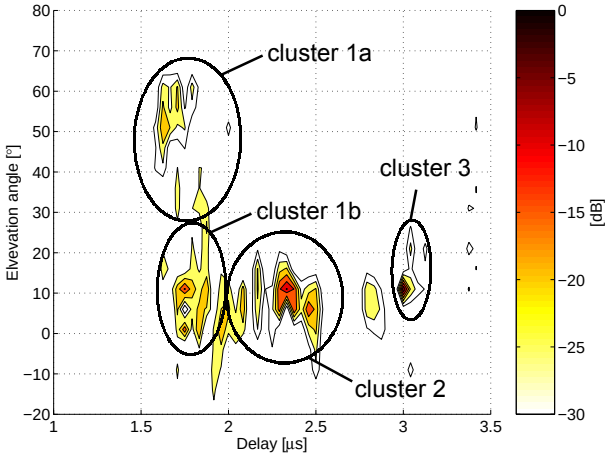

Figure 16. Elevation-delay-power profile at *mobile station*

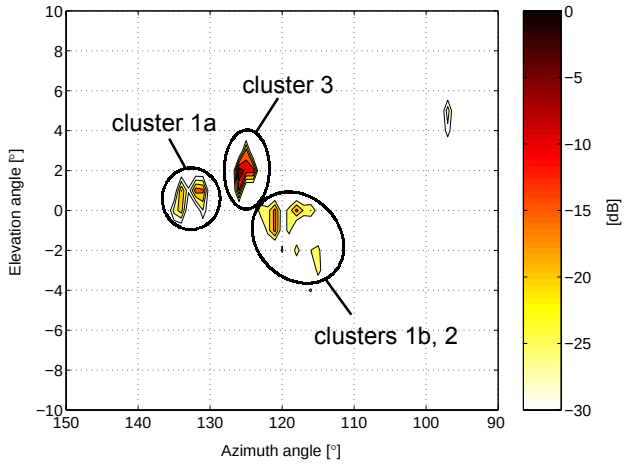

Figure 17. Azimuth-elevation-power profile at *base station*.

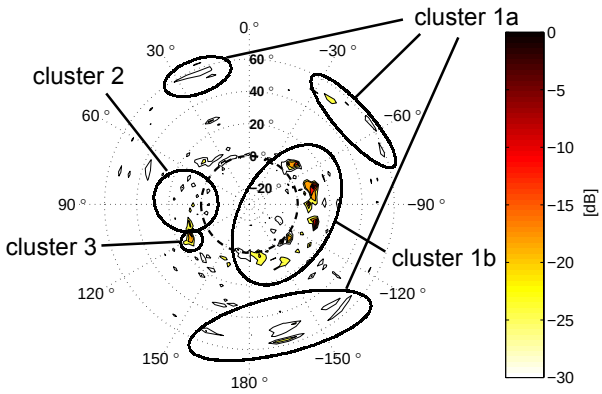

Figure 18. Azimuth-elevation-power profile at *mobile station*

The average power-delay profile in Fig. 12 shows that the propagation paths are concentrated in three delay clusters, with propagation delay ranges of approximately from 1.5 to 1.9 μs, from 2.2 to 2.5 μs, and around 3 μs. However, Figure 13 reveals that the first delay cluster actually consists of two separate azimuth clusters (’cluster 1a’ and ’cluster 1b’ in Figure 13), and thus the total number of propagation clusters is four. The propagation paths corresponding to these clusters are marked in the map of Fig. 11. The cluster boundaries in Figs. 13-18 are not exact.

At the base station the multipaths belonging to ’cluster 1a’ are received from an azimuth window between 130° and 135°. The shortest-delayed component arrives slightly above horizontal plane from 132° in azimuth. The mobile is at 131°. Meanwhile at the mobile station the shortest-delayed multipath arrives from the direction of −160° in azimuth (see Fig. 14) and at a high elevation angle: between 50° and 60° above horizon (see Fig. 16). Based on the intersection point of these two paths it is interpreted that ’cluster 1a’ corresponds to propagation over the rooftop and coupling to street level from the roof-edge of the 38-meter high building next to the mobile station (see Fig. 11). There is a LOS from the base station to the metal roof of the building. High-elevated components are observed also from the opposite side of the street (see Fig. 18), corresponding to secondary reflections from the building wall.

The other short-delayed cluster (’cluster 1b’) arrives at the base station from azimuth angle of approximately 120°. It is assumed that the propagation takes place on street level via the street canyons of ’Keskuskatu street’ and ’Kaisaniemenkatu street’. At the mobile station the first delay cluster can not be further separated in azimuth. Most of the multipath components belonging to this cluster arrive from the direction of the street canyon at right, but multiple reflections from the surrounding walls are visible also from other directions. The multipaths of 'cluster 2' arrive at the mobile station from the opposite direction, and they are assumed to have reflected from the wall of the 31-m high building after first propagating over the roof of the 24-m high building (see Fig. 11). At the base station 'cluster 2' is centered around azimuth angle of 120° (see Fig. 13), which supports the assumption. The third and longest-delayed cluster ('cluster 3') is the strongest one. It corresponds to a single reflection from a building

that rises clearly above the surroundings and has a LOS to both the mobile and base stations. The measured propagation delay and DoAs at both ends agree very well with the geometry.

The presented result well describes a typical propagation scenario where propagation over building roofs occurs. For most of the measured mobile locations, the waves arriving to the mobile from high elevation angles originated from high buildings with LOS to the base station. The components diffracted directly over the rooftop from the direction of the BS were mostly weak, and in many cases they did not exist at all. At the base station site the multipaths were received from a few dominant azimuth angles corresponding to the directions of high-rising buildings in the area, and directly through street canyons for mobile locations at closer distances from the base station.

The two examples presented above show that already visual inspection of the results of spatial radio channel measurements gives general insight into dominant propagation mechanisms in urban environment. In addition, identification of individual propagation path allows investigating the relative strength of various reflecting, scattering, and diffracting contributions. This information is highly useful in evaluation and further development of existing deterministic site-specific propagation models, such as ray tracing tools.

5.2 ANGULAR POWER DISTRIBUTION AT MOBILE STATION

5.2.1 Mean effective gain

Following the analysis by Yeh in [94], Taga in [24] derived a useful expression for the mean effective gain (MEG) of a mobile terminal antenna using the 3-D power gain pattern of the antenna and the angular power distribution in a multipath environment, both defined separately for the θ- and ϕ-polarized components of the incident electrical field. The MEG as the ratio of the power received by an antenna and the total received power is written as:

$$G_e = \oint_{\phi}\oint_{\theta}\left[\frac{P_\theta}{P_\theta + P_\phi} G_\theta(\theta,\phi) p_\theta(\theta,\phi) + \frac{P_\phi}{P_\theta + P_\phi} G_\phi(\theta,\phi) p_\theta(\theta,\phi)\right]\cos\theta d\theta d\phi \tag{5.1}$$

In (5.1), G_θ and G_ϕ are the θ- and ϕ-polarized components of the antenna power gain pattern, respectively. Terms $\frac{P_\theta}{P_\theta + P_\phi}$ and $\frac{P_\phi}{P_\theta + P_\phi}$ are the average portions of the total incident power that would be received by isotropic θ- and ϕ-polarized antennas. In the case of a θ-polarized transmitter antenna, these terms can be written also as a function of the cross-polarization power ratio (XPR) [24], which is then defined as the ratio $\frac{P_\theta}{P_\phi}$. $p_\theta(\theta,\phi)$ and $p_\phi(\theta,\phi)$ are the θ- and ϕ-polarized components of the normalized angular power distributions that satisfy the following condition [94]:

$$\oint_{\phi}\oint_{\theta} p_\theta(\theta,\phi)\cos\theta d\theta d\phi = \oint_{\phi}\oint_{\theta} p_\phi(\theta,\phi)\cos\theta d\theta d\phi = 1 \tag{5.2}$$

In addition, the power gain patterns of the antenna are subject to:

$$\oint_{\phi}\oint_{\theta}\left[G_{\theta}(\theta,\phi)+G_{\phi}(\theta,\phi)\right]\cos\theta d\theta d\phi = \eta_{tot}\,4\pi \tag{5.3}$$

In (5.3) η_{tot} is the total antenna efficiency [95]. It must be noted that in the case of handset antennas measured in [P6], also the dielectric losses due to the human head model are included in η_{tot}. The spherical coordinate system is defined in Fig. 1 of [P6].

In the case of a pedestrian mobile terminal user moving randomly in any environment, the orientation of the mobile antenna in azimuth is random and it is straightforward to assume that the incident waves can arise from any azimuth direction with equal probability. In this case the power distribution in azimuth is uniform and independent of elevation, and the normalized angular power distribution reduces to:

$$p(\theta,\phi)=\frac{1}{2\pi}p(\theta) \tag{5.4}$$

where

$$\oint_{\theta} p(\theta)\cos\theta d\theta = 1 \tag{5.5}$$

It must be noted that the assumption of uniform azimuth power distribution may not be valid for vehicular mounted terminal antennas that tend to follow deterministic routes with well-defined orientations. In such case the effective azimuth power distributions would resemble more those presented in Fig. 3 of [P6]. In this case either the independence of azimuth and elevation would not be obvious. Unlike the azimuth, no straightforward assumption can be justified for the elevation power distribution in elevation in any case.

5.2.2 Computation of angular power distributions and XPR from measurement data

As a result of the analysis described in Sec. 4.3.3, the θ- and ϕ-polarized components of the angle resolved impulse response – $h_{\theta,i}(\theta,\phi,\tau)$ and $h_{\phi,i}(\theta,\phi,\tau)$ defined in Eq. (5) of [P6] – were obtained for each measurement snapshot. The azimuth and elevation power distributions were derived from the angle resolved impulse response using the following formulas (presented in different form in Table 1 of [P6]). First the instantaneous power as a function of azimuth or elevation angle was computed as a sum of the multipath powers over all possible delay and angle values:

$$\begin{aligned} P_{\theta,i}(\phi) &= \sum_{\tau}\sum_{\theta}\left|h_{\theta,i}(\theta,\phi,\tau)\right|^2 & P_{\theta,i}(\theta) &= \sum_{\tau}\sum_{\phi}\left|h_{\theta,i}(\theta,\phi,\tau)\right|^2 \\ P_{\phi,i}(\phi) &= \sum_{\tau}\sum_{\theta}\left|h_{\phi,i}(\theta,\phi,\tau)\right|^2 & P_{\phi,i}(\theta) &= \sum_{\tau}\sum_{\phi}\left|h_{\phi,i}(\theta,\phi,\tau)\right|^2 \end{aligned} \tag{5.6}$$

Then the instantaneous portions of θ- and ϕ-polarized powers of the total incident power as a function of azimuth and elevation angles in one environment were computed and averaged over all measurement snapshots in the environment:

$$\frac{P_\theta}{P_\theta + P_\phi} p_\theta(\phi) = \frac{1}{N}\sum_{i=1}^{N} \frac{P_{\theta,i}(\phi)}{P_i} \qquad \frac{P_\theta}{P_\theta + P_\phi} p_\theta(\theta) = \frac{1}{N}\sum_{i=1}^{N} \frac{P_{\theta,i}(\theta)}{P_i}$$
$$\frac{P_\phi}{P_\theta + P_\phi} p_\phi(\phi) = \frac{1}{N}\sum_{i=1}^{N} \frac{P_{\phi,i}(\phi)}{P_i} \qquad \frac{P_\phi}{P_\theta + P_\phi} p_\phi(\theta) = \frac{1}{N}\sum_{i=1}^{N} \frac{P_{\phi,i}(\theta)}{P_i} \tag{5.7}$$

The normalization is such that the integrals of $p(\phi)$ and $p(\theta)$ in Eq. (5.7) are equal to unity. The instantaneous total incident power equals to:

$$P_i = \sum_\tau \sum_\theta \sum_\phi \left[\left| h_{\theta,i} \right|^2 + \left| h_{\phi,i} \right|^2 \right] \tag{5.8}$$

It is noted that most probably the angular θ- and ϕ-polarized power distributions are not stationary processes for measurement routes of hundreds of meters of length. However, as an engineering tool the proposed computation method should lead to fair comparison between handset antennas in realistic usage environments. Due to the large measurement bandwidth compared to the channel coherence bandwidth the fast fading of the total received power (sum of the multipath powers) was small. The distribution of the square root of the total power relative to the local mean power (averaged over a distance of approximately 30 wavelengths) agreed well with Rice distribution and the average fitted Rice factor varied from k≈17 in the outdoor-indoor case to k≈60 in the urban macrocell case. Thus the total incident power measured with the spherical array approximates well the sum of wideband powers that would be received by isotropic θ- and ϕ-polarized antennas, if such existed.

In the case of vertically (θ-) polarized transmission, the XPR is defined as the power ratio of θ- and ϕ-polarized components of the mean incident field. The XPR was obtained from the measurement data as the ratio of the average θ- and ϕ-polarized portions of the total incident power:

$$XPR = \frac{P_\theta}{P_\theta + P_\phi} \Big/ \frac{P_\phi}{P_\theta + P_\phi} \tag{5.9}$$

5.2.3 Elevation power distribution

Figure 19 shows two examples of measured elevation power distributions (EPDs) in urban environment.

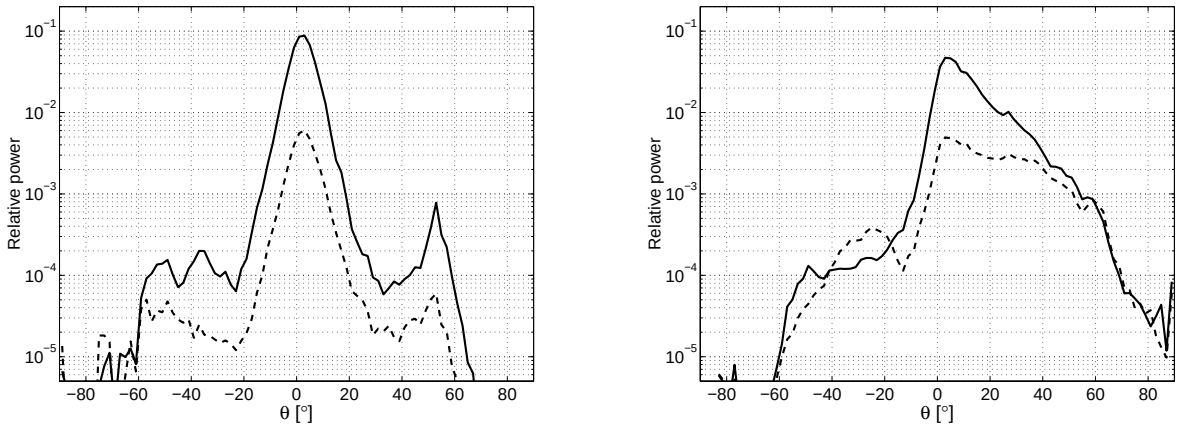

Figure 19. Elevation power distribution at mobile station [P6]. (a) urban microcell, h_{BS}=8 m. (b) urban macrocell, h_{BS} =27 m. Thick and thin lines correspond to θ- and ϕ-polarized distributions, respectively.

It was found in the measurements described in [P6] that in NLOS situations the EPD has a shape of a double-sided exponential function, with different slopes on the negative and positive sides of the peak. The slopes and the peak elevation angle depend on the environment type and base station antenna height. It was further noticed that the power distribution becomes asymmetrical when the BS antenna is raised above the rooftop level in urban environment. For lower BS antenna heights the power is concentrated only slightly above the horizontal plane.

5.2.4 Angle-delay power spectra

Stochastic spatial channel models rely on realistic geometrical scatterer distributions at the mobile and base stations. The following examples present the measured distribution of incident power over delay and angle dimensions at the mobile station, and thus represent the scatterer distribution as it is seen by a mobile antenna. In addition, the relative portion of power received from high elevation angles describes the significance of propagation over building rooftops in different environments.

Based on measurements reported in [P5], the average angle-delay power spectra for elevation and azimuth in urban macrocell environment are presented in Figs. 20 and 21, respectively. By employing the measurement technique based on spherical antenna array it was possible to collect a large amount of data; the total number of angle resolved impulse responses included in the average spectra is over 100 000, and they were collected along 2.5 km of measurement routes. The variation of the received power was removed before averaging by normalizing the spectra to the total received power for each impulse response. The delay is referenced to the first received multipath at each point; i.e. it is the excess delay.

The shape of the elevation-delay power spectrum in Fig. 20 demonstrates how the energy propagating above rooftops is coupled to street level with short excess delays. Propagation along street canyons dominates for excess delays larger than 1 μs, which can be seen as low elevation angles. The maximum of the elevation-delay power spectrum is found at an eleva-

tion angle of 7° and at excess delay of 0.3 µs. The azimuth-delay power spectrum of Fig. 21 shows that for short excess delays the power spreads almost equally in all azimuth directions, but at an excess delay of approximately 0.4 µs certain directions begin to dominate. Longest-delayed multipaths are received from the directions of the street canyon (0°, 180°), but also the effect of crossing streets can be seen as longer delays around azimuth angles of ±90°. Similar type of scattering distribution in azimuth was observed also by Kuchar et al. in a quite different city [30], even with the same breakpoint value of 0.4 µs.

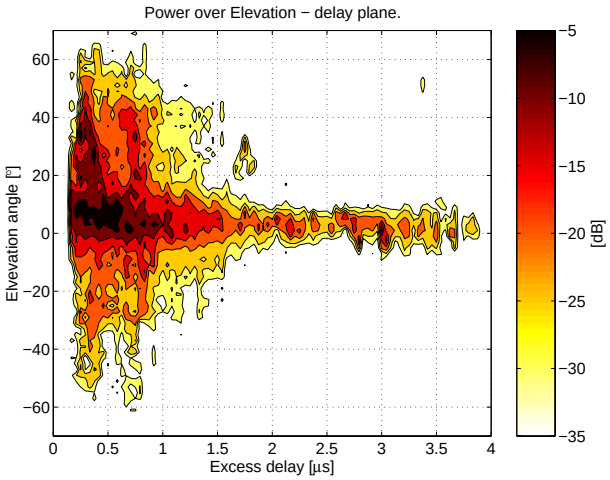

Figure 20. Elevation-delay power spectrum in urban macrocell.

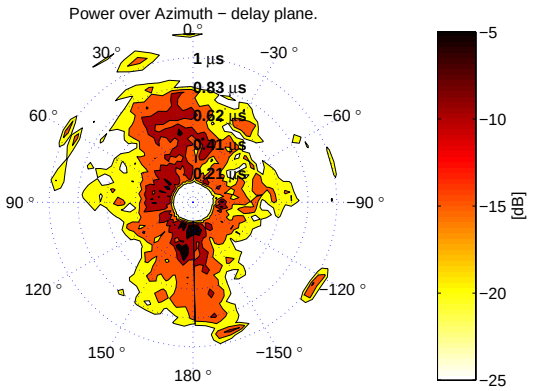

Figure 21. Azimuth-delay power spectrum in urban macrocell. Angles 0° and 180° are parallel to street canyon.

5.3 POLARIZATION CROSS COUPLING

The polarization of the electrical field radiated by an antenna depends on the orientation and geometry of the antenna (and on the angle of observation). The physical propagation phenomena, i.e. diffraction, reflection, refraction, are polarization-dependent, and thus in the radio channel part of the energy is coupled to polarization orthogonal to the transmitted polarization. This is referred to as polarization cross coupling [53]. The polarization cross coupling is written as:

$$\Gamma = \frac{P_1}{P_1 + P_2} = \frac{1}{1 + \frac{P_2}{P_1}} = \frac{1}{1 + XPR} \tag{5.10}$$

In (5.10) P_1 and P_2 are the received cross- and co-polarized powers, respectively. The ratio P_2/P_1 equals to the XPR. The polarization properties of the received electrical field at the mobile station were analyzed in [P5] based on experimental data from different radio environments. Figure 22 presents a probability plot for the polarization cross coupling measured using the spherical array in urban microcell environment with measurement distances in the range of 50…450 m (22 % LOS, 78 % NLOS). The dash-dotted line shows a lognormal distribution fitted to the data. It can be observed that the experimental data agrees well with the lognormal reference for probability levels between 10 % and 98 %. In the presented case the

median, mean, and standard deviation of the instantaneous polarization cross coupling are –12.7 dB, –12.9 dB, and 3.4 dB, respectively. It must be noted that for small polarization cross coupling (high XPR) the uncertainty of the measurement is increased due to the finite XPD of the spherical array.

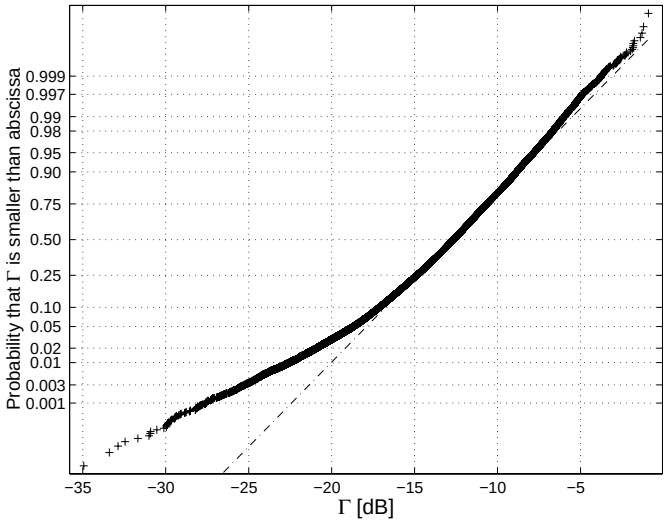

Figure 22. Polarization cross coupling in urban microcell, h_{BS} = 8 m, measurement distances in the range from 50 m to 450 m, portion of LOS measurements 22 %.

The portion of electromagnetic energy that is lost due to polarization mismatch depends on the relative orientations of the transmitter and receiver antennas, and on the polarization cross coupling in the radio channel. Sometimes the polarization of one of the antennas is unknown, which is the case with mobile handset antennas, whose polarization properties depend on how the user holds the handset. In [P6] it was found that the mean polarization cross coupling was between –7 and –12 dB (XPR between 6 and 12 dB) in all measured environments. The rather low coupling indicates that it would be beneficial to optimize the polarization of the cellular radio link by using a transmission antenna with adaptive polarization properties at the base station. Such polarization matching concept has been recently proposed in [96].

6. SUMMARY OF PUBLICATIONS

Paper [P1] presents a novel measurement method for the real-time acquisition of radio channel data with multiple antennas, employing a single radio receiver. The system is based on a wideband radio channel sounder and a fast RF multiplexer. The performance of the system is described and the used method for extracting the DoA information from data recorded with an antenna array is explained in detail. The functionality of the system is demonstrated with practical measurements using a linear 8-element antenna array in suburban and urban environments. Especially the urban measurement gives a very interesting result by showing the large angular dispersion of the microcellular environment with both antennas below the building rooftop level.

In [P2], a new measurement concept enabling the complete real-time characterization of the wideband mobile radio channel is presented. The concept is based on a spherical antenna array, and it provides directional information of the incident waves over the full 4π solid angle. The geometry and construction of the spherical array is described in detail, and two methods for extracting the DoA information are evaluated. The directional properties of the measurement system including angular resolution, angular dynamic range, cross polarization discrimination, accuracy of measured incidence angle, and amplitude and phase ripple vs. incidence angle are defined with test measurements in an anechoic chamber.

Paper [P3] describes 3-D radio channel measurements at the base station in urban environment, combining the RF-switched receiver array and the synthetic aperture technique, and allowing full 3-D characterization of the channel. Dual-polarized patch antennas as array elements enable determination of the polarization properties of the impinging waves. The azimuth and elevation angles of the incident waves are estimated using a high-resolution 2-D Unitary ESPRIT algorithm. Measurements at over 70 different transmitter positions and three receiver array sites with different sectors and antenna heights are presented. The results show that the received energy is concentrated within identifiable clusters in the azimuth-elevation-delay domain. It is demonstrated that the environment close to the base station mainly determines the observed propagation mechanisms. Street canyon propagation dominates also when the receiver array is at or even above rooftop level with the studied distances up to 500 m. Multipaths propagating over the rooftop are mainly related to reflections from high-rise buildings in the surroundings. The azimuth spectrum at the BS site is fairly independent of the location of the mobile, which indicates that at a site of this kind interference rejection by spatial filtering would not be as efficient as in a more open radio environment.

In paper [P4], the experimental data presented in [P3] is examined in more detail, by analyzing such properties of the radio channel that have an effect on the performance of a beamforming base station antenna. It is found that in 90 % of the cases pointing a single antenna beam (VP, beamwidth $\geq 23°$) towards the strongest cluster in azimuth causes a loss of no more than 2.6 dB of the total incident power. Over 90 % of the total power is concentrated in the strongest cluster for the base station site dominated by a wide approaching street. In average the number of clusters at the base station (defined by visual inspection) was 3.8, while the maximum was 8. The cluster powers showed an exponential decay vs. delay of approximately

8.9 dB/μs, and the standard deviation from the exponential law is independent of the cluster excess delay. The average cross polarization power ratio was 8.0 dB, and it was found that the coupling from the transmitted vertical to received horizontal polarization was stronger for propagation over building rooftops than along street canyons: the difference in the XPR values was 5 dB.

Paper [P5] describes extensive 3-D directional radio channel measurements performed at the mobile station in different radio environments, using the measurement technique described in [P2]. Both average and instantaneous angular distributions of incident power along long continuous routes are presented. The instantaneous power distributions show that a few dominant secondary sources with long lifetimes exist both in urban macrocell and microcell types of propagation environments. Also diffuse scattering from local surroundings of the mobile exists. The results of continuous directional channels are first of their kind in the literature, and they clearly demonstrate the usefulness of the measurements in characterizing radio propagation in difficult radio environments.

Paper [P6] presents experimental results of the elevation power distribution and XPR in different radio environments. Two parameterized models for the EPD are evaluated, and the fitted parameter values of both models in each environment are presented. The results show that in NLOS situations the power distribution in elevation has a shape of a double-sided exponential function, with different slopes on the negative and positive sides of the peak. The slopes and the peak elevation angle depend on the environment and base station antenna height. The XPR varies within 6.6 and 11.4 dB, being lowest for indoor, and highest for urban microcell environments, where street canyon propagation dominates. Lowest XPR values correspond to waves received from high elevation angles, corresponding to propagation over building rooftops. The experimental data are applied for analysis of the mean effective gain of several mobile handset antennas. The results show that considering only the efficiency of the antenna is not enough to describe its performance in practical operation environments. For most antennas the environment has little effect on the MEG, but clear differences exist between antennas. The MEG also depends on which side of the head the user holds the handset.

7. CONCLUSIONS

In this thesis new systems for multidimensional measurements of the multipath mobile radio channel were developed and applied to extensive measurements in practical propagation environments.

The HUT/IDC radio channel sounder was extended for fast multiple output channel measurements at frequencies up to 18 GHz, by applying RF switching. The data acquisition system of the sounder was developed to enable high data rates corresponding to continuous real-time storage of wideband radio channel data from multiple antenna elements. Two dual-polarized antenna arrays were built for measuring the 3-D multipath radio channel at both the base and mobile stations of a cellular communication link at 2 GHz.

The functionality of the developed measurement techniques was proved and their usefulness demonstrated by performing extensive radio channel measurements at 2 GHz and analyzing the experimental data. Spatial channels of both the mobile and base stations were analyzed, as well as the double-directional channel that fully characterizes the propagation between two antennas. Based on identification of the last scattering objects before the wave reaches the antennas it was possible to track the entire propagation history of the strongest multipath components. It was shown that already visual inspection of the data gives insight into dominant radio propagation mechanisms in such radio environments where their prediction is difficult.

In urban macrocell measurements it was observed that typically the multipath components arriving to the mobile from high elevation angles originated from high buildings with LOS to the base station. The components diffracted directly over the rooftop from the direction of the base station were mostly weak, and in many cases they did not exist at all. At the base station site the waves were received from a few dominant azimuth angles corresponding to the directions of high-rising buildings in the area, and directly through street canyons for mobile locations at closer distances from the base station.

According to measurements at the mobile station in urban environment, the power solely propagates along street canyons when the BS antenna is located below the mean rooftop level. In elevation domain the incident power at the mobile station is concentrated close to the horizontal plane independently of the base station antenna height. The elevation power distribution has a shape of a double-sided exponential function, with different slopes on the negative and positive sides of the peak. Coupling of energy from transmitted vertical to received horizontal polarization is of the order of -10 dB for lateral (street level) propagation. The coupling is stronger for multipaths propagated over building rooftops.

Conventional angular domain measurement techniques require static channel conditions. This restriction makes them slow and thus infeasible for collecting large amounts of data for tuning of stochastic channel models. Furthermore, they fail to capture the Doppler dimension of the channel. Unlike the conventional ones, the measurement techniques presented in this thesis are unique in that they enable continuous radio channel measurements at practical mobile speeds including all channel dimensions: direction, time, frequency, and polarization. In addi-

tion, properties of both small and large scale fading of the channel can be derived from measurements performed over long continuous routes.

Profound knowledge of radio propagation in diverse multipath environments is essential for the successful implementation of future radio communication systems exploiting spatial processing, such as MIMO systems. The measurement techniques presented in this thesis contribute to improving the understanding of the dominant radio propagation mechanisms in complex environments. They also provide means for collecting realistic data for accuracy evaluation of existing deterministic propagation models as well as for parameter extraction for stochastic spatial channel models.

Errata

In [P2] in third paragraph of page 440. Doppler spectrum of each wave should read Doppler shift of each wave.

REFERENCES

[1] Web page of GSM Association. Available in <URL: http://www.gsmworld.com/>. Last updated in January 9, 2002 [cited January 10, 2001].

[2] H. Holma, A. Toskala, *WCDMA for UMTS*, Wiley, New York, 2001, 313 p.

[3] European Telecommunications Standards Institute (ETSI), Broadband Radio Access Networks (BRAN), "HIPERLAN Type 2 Functional Specification Part 1 - Physical (PHY) layer," 1999.

[4] L. M. Correia (ed.), *Wireless Flexible Personalised Communications, COST 259: European Co-operation in Mobile Radio Research*, Wiley, March 2001, 512 p.

[5] Web page of COST Action 273: "Towards Mobile Broadband Multimedia Networks". Available in <URL: http://www.lx.it.pt/cost273/>. Last updated in January 2, 2002 [cited January 10, 2002].

[6] A. J. Paulraj, C. B. Papadias, "Space-time processing for wireless communications, improving capacity, coverage, and quality in wireless networks by exploiting the spatial dimension," *IEEE Signal Processing Magazine*, vol. 14, no. 5, pp. 49-83, November 1997.

[7] G. J. Foschini and M. J. Gans, "On limits of wireless communication in a fading environment when using multiple antennas," *Wireless Personal Communications*, vol. 6, no. 3, pp. 311–335, March 1998.

[8] C. B. Dietrich, Jr., W. L. Stutzman, K. Byung-Ki, K. Dietze, "Smart antennas in wireless communications: base station diversity and handset beamforming," *IEEE Antennas and Propagation Magazine,* vol. 42, no. 5, pp. 142-151, October 2000.

[9] L. C. Godara, "Application of antenna arrays to mobile communications, Part II: Beamforming and direction-of-arrival considerations," *Proceedings of the IEEE,* vol. 85, no. 8, pp. 1195-1245, August 1997.

[10] J. H. Winters, "The diversity gain of transmit diversity in wireless systems with Rayleigh fading," *IEEE Transactions on Vehicular Technology,* vol. 47, no. 1, pp. 119-123, February 1998.

[11] J. Laurila, *Semi-Blind Detection of Co-Channel Signals in Mobile Communications*, Doctoral Thesis, the Finnish Academies of Technology, 2000, 166 p.

[12] H. Krim and M. Viberg, "Two decades of array signal processing research: the parametric approach," *IEEE Signal Processing Magazine,* vol. 13, no. 4, pp. 67-94, July 1996.

[13] R. B. Ertel, P. Gardieri, K. Sowerby, T.S. Rappaport, and J.H. Reed, "Overview of spatial channel models for antenna array communication systems," *IEEE Personal Communications*, vol. 5, no. 1, pp. 10-22, February 1998.

[14] B. H. Fleury and P. E. Leuthold, "Radiowave propagation in mobile communications: an overview of european research," *IEEE Communications Magazine*, vol. 34, no. 2, pp. 70-81, February 1996.

[15] J. Bach Andersen, T. S. Rappaport, and S. Yoshida, "Propagation measurements and models for wireless communications channels," *IEEE Communications Magazine,* vol. 33, no. 1, pp. 42-49, January 1995.

[16] A. M. Vernon, M. A. Beach, and J. P. McGeehan, "Planning and optimisation of smart antenna base stations in 3G networks," *Proceedings of IEE Colloquium on Capacity and Range Enhancement Techniques for the Third Generation Mobile Communications and Beyond (Ref. No. 2000/003),* 11 February, 2000, pp. 1/1-1/7.

[17] U. Martin, J. Fuhl, I. Gaspard, M. Haardt, A. Kuchar, C. Math, A. F. Molisch, and R. Thomä, "Model scenarios for intelligent antennas in cellular mobile communication systems - scanning the literature," *Wireless Personal Communications Magazine, Special Issue on Space Division Multiple Access,* vol. 11, no. 1, pp. 109-129, November 1999.

[18] E. Damosso and L. Correia (eds.), *Digital Mobile Radio Towards Future Generation Systems, COST 231 Final Report,* Europan Commission, 1999, 474 p.

[19] H. L. Bertoni, *Radio Propagation for Modern Wireless Systems,* Prentice Hall PTR, New Jersey, USA, 2000, 258 p.

[20] N. Blaunstein, *Radio Propagation in Cellular Networks,* Artech House, Boston, 2000, 386 p.

[21] J. Syrjärinne, *Studies of modern techniques for personal positioning*, Doctoral Thesis, Tampere University of Technology, 2001, 180 p.

[22] D. Kothris, M. Beach, B. Allen, and P. Karlsson, "Performance assessment of terrestrial and satellite based position location systems," *Proceedings of 2nd International Conference on 3G Mobile Communication Technologies,* 26-28 March, 2001, pp. 211-215.

[23] Web page of Mobile Location Technologies of VTT Information Technology. Available in <URL: http://location.vtt.fi>. Last updated in September 4, 2001 [cited January 10, 2002].

[24] T. Taga, "Analysis for mean effective gain of mobile antennas in land mobile radio environments," *IEEE Transactions on Vehicular Technology*, vol. 39, no. 5, pp. 117-131, May 1990.

[25] G. F. Pedersen and J. Bach Andersen, "Handset antennas for mobile communications: integration, diversity, and performance," Chapter 5 in *Review of Radio Science 1996-1999,* editor W.R. Stone, Oxford, Oxford University Press, 1999, 970 p.

[26] U. Martin, "Spatio-temporal radio channel characteristics in urban macrocells," *IEE Proceedings on Radar, Sonar and Navigation,* vol. 145, no. 1, pp. 42-49, February 1998.

[27] P. Pajusco, "Experimental characterization of DOA at the base station in rural and urban area," *Proceedings of 48th IEEE Annual Vehicular Technology Conference,* Ottawa, Ontario, Canada, May 18-21, 1998, pp. 993-997.

[28] K. I. Pedersen, P. E. Mogensen, and B. H. Fleury, "Spatial channel characteristics in outdoor environments and their impact on BS antenna system performance," *Proceedings of 48th IEEE Annual Vehicular Technology Conference,* Ottawa, Ontario, Canada, May 18-21, 1998, pp. 719-723.

[29] J. Fuhl, J.-P. Rossi, and E. Bonek, “High-resolution 3-D direction-of-arrival determination for urban mobile radio,” *IEEE Transactions on Antennas and Propagation*, vol. 45, no. 4, pp. 672-682, April 1997.

[30] A. Kuchar, J.-P. Rossi, and E. Bonek, “Directional macro-cell channel characterization from urban measurements,” *IEEE Transactions on Antennas and Propagation,* vol. 48, no. 2, pp. 137-146, February 2000.

[31] H. Laitinen, K. Kalliola, and P. Vainikainen, “Angular signal distribution and cross-polarization power ratio seen by a mobile receiver at 2.15 GHz,” *Proceedings of Millennium Conference on Antennas & Propagation (AP2000),* Davos, Switzerland, April 9-14, 2000, CD-ROM SP-444 (ISBN 92-9092-776-3), paper p1133.pdf.

[32] J.-P. Rossi, J.-P. Barbot, and A. J. Levy, “Theory and measurement of the angle of arrival and time delay of UHF radiowaves using a ring array,” *IEEE Transactions on Antennas and Propagation*, vol. 45, no. 5, pp. 876-884, May 1997.

[33] Y. L. C. de Jong, M. H. A. J. Herben, “High-resolution angle-of-arrival measurement of the mobile radio channel,” *IEEE Transactions on Antennas and Propagation*, vol. 47, no. 11, pp. 1677-1687, November 1999.

[34] T. S. Rappaport, *Wireless Communications, Principles and Practice,* Prentice Hall, Upper Saddle River, 1996, 641 p.

[35] S. R. Saunders, *Antennas and Propagation for Wireless Communication Systems,* Wiley, New York, 1999, 409 p.

[36] R. G. Kouyoumjian and P. H. Pathak, “A uniform theory of diffraction for an edge in pefectly conducting surface,” *Proceedings of IEEE,* vol. 62, pp. 1448-1461, November 1974.

[37] R. J. Luebbers, “A heuristic UTD slope diffraction coefficient for rough lossy wedges,” *IEEE Transactions on Antennas and Propagation,* vol. 37, no. 2, pp. 206-211, February 1989.

[38] P. D. Holm, “A new heuristic UTD diffraction coefficient for nonperfectly conducting wedges,” *IEEE Transactions on Antennas and Propagation,* vol. 48, no. 8, pp. 1211-1219, August 2000.

[39] A. T. Alastalo, A. Väisänen, K. Leppänen, K. Kalliola, M. E. Ermutlu, and A. Brehonnet, “Adaptive Antennas for Wireless Local Area Networks,” *Proceedings of Millennium Conference on Antennas & Propagation (AP2000),* Davos, Switzerland, April 9-14, 2000, CD-ROM SP-444 (ISBN 92-9092-776-3), paper p1102.pdf.

[40] M. Hata, “Empirical formulae for propagation loss in land mobile radio sercvices,” *IEEE Transactions on Vehicular Technology,* vol. 29, pp. 317-325, 1980.

[41] J. Walfisch and H. L. Bertoni, “A theoretical model for UHF propagation in urban environments,” *IEEE Transactions on Antennas and Propagation,* vol. 36, no. 12, pp. 1788-1796, December 1988.

[42] F. Ikegami, T. Takeuchi, and S. Yoshida, “Theoretical prediction of mean field strength for urban mobile radio,” *IEEE Transactions on Antennas and Propagation,* vol. 39, no. 3, pp. 299-302, March 1991.

[43] D. Har, A. M. Watson, and A. G. Chadney, "Comment on diffraction loss of rooftop-to-street in COST 231-Walfisch–Ikegami model," *IEEE Transactions on Vehicular Technology,* vol. 48, no. 5, September 1999, pp. 1451-1452.

[44] M. F. Cátedra, J. Pérez-Arriaga, *Cell Planning for Wireless Communications,* Artech House, Boston, 1999, 199 p.

[45] K. A. Remley, A. Weisshaar, and H. R. Anderson, "A comparative study of ray tracing and FDTD for indoor propagation modeling," *Proceedings of 48th IEEE Annual Vehicular Technology Conference,* Ottawa, Ontario, Canada, May 18-21, 1998, pp. 865-869.

[46] S.-C. Kim, B.J. Guarino, Jr., T. M. Willis III, V. Erceg, S. J. Fortune, R. A. Valenzuela, L. W. Thomas, J. Ling, and J. D. Moore, "Radio propagation measurements and prediction using three-dimensional ray tracing in urban environments at 908 MHz and 1.9 GHz," *IEEE Transactions on Vehicular Technology,* vol. 48, no. 3, pp. 931-946, May 1999.

[47] M. Failli (ed.), *Digital Land Mobile Communications, COST 207 Final Report,* 1989.

[48] V. Perez (ed.), "Final propagation model," Rep. R2020/TDE/PS/DS/P/040/al, RACE UMTS Code Division Testbed (CODIT), June 1994.

[49] R. Gollreiter (ed.), "Channel models," Rep. R2084/ESG/CC3/DS/P/029/bl, RACE Advanced TDMA Mobile Access (ATDMA), May 1994.

[50] R. Heddergott, U.P. Bernhard, and B.H. Fleury, "Stochastic radio channel model for advanced indoor mobile communication systems," *Proceedings of 8th IEEE International Symposium on Personal, Indoor and Mobile Radio Communications,* Helsinki, Finland, September 1-4, 1997, pp. 140-144.

[51] R. H. Clarke, "A statistical theory of mobile radio reception," *Bell. Syst. Tech. Journal*, Vol. 47, July/Aug. 1968, pp. 957-1000.

[52] J. Fuhl, A. F. Molisch, and E. Bonek, "A unified channel model for mobile radio systems with smart antennas," *IEEE Proceedings on Radar, Sonar and Navigation: Special Issue on Antenna Array Processing Techniques*, vol. 145, no. 1, pp. 32-41, February 1998.

[53] W. C.-Y. Lee and Y. S. Yeh, "Polarization diversity system for mobile radio," *IEEE Transactions on Communications*, vol. COM-20, no. 5, pp. 912–923, October 1972.

[54] J. D. Parsons, D. A. Demery, and A. M. D. Turkmani, "Sounding techniques for wideband mobile radio channels: a review," *IEE Proceedings-I,* vol. 138, no. 5, pp. 437-446, October 1991.

[55] J. Kivinen, T. Korhonen, P. Aikio, R. Gruber, P. Vainikainen, and S.-G. Häggman, "Wideband radio channel measurement system at 2 GHz," *IEEE Transactions on Instrumentation and Measurement*, vol. 48, no. 1, pp. 39-44, February 1999.

[56] A. Hewitt, "Selective Fading on LOS Microwave Links: Classical and Spread-Spectrum Measurement Techniques," *IEEE Transactions on Communications*, vol. 36, no. 7, pp. 789-796, July 1988.

[57] T. Korhonen and S.-G. Häggman, "Location of subchip radio channel multipath Components from direct sequence sounding data," *Proceedings of IEEE International Con-*

ference on Personal Wireless Communications, December 17-20, 1997 Bombay, India, pp. 43-47.

[58] B. H. Fleury, M. Tschudin, R. Heddergott, D. Dahlhaus, and K. I. Pedersen, "Channel parameter estimation in mobile radio environments using the SAGE algorithm," *IEEE Journal on Selected Areas in Communications,* vol. 17, no. 3, pp. 434-450, March 1999.

[59] R. McDonough, *Detection of Signals in Noise,* Second Edition, Academic Press, USA, 1995, 495 p.

[60] C. Ward, M. Smith, A. Jeffries, D. Adams, and J. Hudson, "Characterising the radio propagation channel for smart antenna systems," *Electronics & Comm. Eng. Journal*, pp. 191-200, August 1996.

[61] A. Klein, W. Mohr, R. Thomas, P. Weber, and B. Wirth, "Direction-of-arrival of partial waves in wideband mobile radio channels for intelligent antenna concepts," *Proceedings of 46th IEEE Annual Vehicular Technology Conference,* Atlanta, Georgia, USA, April 28 - May 1, 1996, pp. 849-853.

[62] J. Laiho-Steffens and A. Wacker, "Experimental evaluation of the two-dimensional mobile propagation environment at 2 GHz," *Proceedings of IEEE 47th Vehicular Technology Conference (VTC'97),* Phoenix, Arizona, USA, May 4-7, 1997, pp. 2070-2074.

[63] J. Kivinen, X. Zhao, and P. Vainikainen, "Wideband indoor radio channel measurement with direction of arrival estimations in the 5 GHz Band", *Proceedings of 50th IEEE Annual Vehicular Technology Conference*, Amsterdam, The Netherlands, September 19-22, 1999, pp. 2308-2312.

[64] J. Ø. Nielsen, G. F. Pedersen, and K. Olesen, "Computation of mean effective gain from 3D measurements," *Proceedings of 49th IEEE Annual Vehicular Technology Conference,* Houston, Texas, USA, May 16-20, 1999, pp. 787-791.

[65] M. B. Knudsen, G. F. Pedersen, B. G. H. Olsson, K. Olesen, and S.-Å. A. Larsson, "Validation of handset antenna test methods," *Proceedings of IEEE 52nd Vehicular Technology Conference (VTC2000-Fall),* Boston, MA, USA, 24-28 September, 2000, vol. 4, pp. 1669-1676.

[66] T. Lo and J. Litva, "Angles of arrival of indoor multipath," *Electronics Letters*, vol. 28, no. 18, pp. 1687-1689, August 1992.

[67] J. G. O. Moss, M. P. Fitton, A. M. Street, K. M. Brown, C. C. Constantinou, and D. J. Edwards, "Spatio-temporal variability analysis of the wideband microcellular environment," *Proceedings of 48th IEEE Annual Vehicular Technology Conference,* Ottawa, Ontario, Canada, May 18-21, 1998, pp. 293-297.

[68] P. E. Mogensen, F. Frederiksen, H. Dam, K. Olesen, and S. L. Larsen, "Tsunami (II) Stand Alone Testbed", *Proceedings of ACTS Mobile Telecommunications Summit*, Granada, Spain, November 27-29, 1996, pp. 517-527.

[69] B. Kim, W. L. Stutzman, and D. G. Sweeney, "Indoor and outdoor measurements of space, polarization, and angle diversity for cellular base stations in urban environments," *Proceedings of IEEE 52nd Vehicular Technology Conference (VTC2000-Fall),* Boston, MA, USA, 24-28 September, 2000, vol. 1, pp. 22-29.

[70] J. Litva, A. Ghaforian, and V. Kezys, "High-resolution measurements of AoA and time-delay for characterizing indoor propagation environments," *Antennas and Propagation Society International Symposium, 1996. AP-S. Digest,* vol. 2, 21-26 July, 1996, pp. 1490-1493.

[71] U. Trautwein, K. Blau, D. Brückner, F. Herrmann, A. Richter, G. Sommerkorn, and R. S. Thomä, "Radio channel measurement for realistic simulation of adaptive antenna arrays," *The 2nd European Personal Mobile Radio Conference*, Bonn, Germany, September 30-October 2, 1997, pp. 491-498.

[72] M. Nilsson, B. Lindmark, M. Ahlberg, M. Larsson, and C. Beckman, "Characterization of a wideband radio channel using spatio temporal polarization measurements," *Proceedings of 10th IEEE International Symposium on Personal, Indoor and Mobile Radio Communications (PIMRC'99),* Osaka, Japan, September 12-15, 1999.

[73] P. H. Lehne, O. Røstbakken, and M. Pettersen, "Estimating smart antenna performance from directional radio channel measurements," *Proceedings of 50th IEEE Annual Vehicular Technology Conference*, Amsterdam, The Netherlands, September 19-22, 1999, pp. 57-61.

[74] B. Allen, J. Webber, P. Karlsson, and M. Beach, "UMTS spatio-temporal propagation trial results," *Proceedings of IEE 11th International Conference on Antennas and Propagation,* vol. 2, 17-20 April, 2001, pp. 497-501.

[75] W. C. Jakes, Y. S. Yeh, M. J. Gans, and D. O. Reudink, "Fundamentals of diversity systems," Chapter 5 in *Microwave Mobile Communications Wireless Communication Systems*, editor W. C. Jakes, New York, John Wiley & Sons, 1974, 642 p.

[76] B. H. Fleury, D. Dahlhaus, R. Heddergott, and M.Tschudin, "Wideband angle of arrival estimation using the SAGE algorithm," *Proceedings of 4th IEEE International Symposium on Spread Spectrum Techniques and Applications*, Mainz, Germany, September 22-25, 1996, pp. 79-85.

[77] K. I. Pedersen, B. H. Fleury, and P. E. Mogensen, "High resolution of electromagnetic waves in time-varying radio channels," *Proceedings of 8th IEEE International Symposium on Personal, Indoor and Mobile Radio Communications,* Helsinki, Finland, September 1-4, 1997, pp. 650-654.

[78] M. D. Zoltowski, M. Haardt, C. Mathews, "Closed-form 2-D angle estimation with rectangular arrays in element space or beamspace via unitary ESPRIT", *IEEE Transactions on Signal Processing*, Vol. 44, No. 2, February 1996, pp. 316-328.

[79] A. Richter and R.S. Thomä, "CUBA-ESPRIT for angle estimation with circular uniform beam arrays", *Proceedings of Millennium Conference on Antennas & Propagation (AP2000),* Davos, Switzerland, April 9-14, 2000, CD-ROM SP-444 (ISBN 92-9092-776-3), paper p1156.pdf.

[80] E. Bonek and M. Steinbauer, "Double-directional channel measurements," *Proceedings of 11th IEE International Conference on Antennas and Propagation (ICAP),* Manchester, UK, April 17-20, 2001.

[81] M. Steinbauer, D. Hampicke, G. Sommerkorn, A. Schneider, A. F. Molisch, R. Thoma, and E. Bonek, "Array measurement of the double-directional mobile radio channel,"

Proceedings of 51st IEEE Vehicular Technology Conference (VTC 2000-Spring), Tokyo, Japan, May 15-18, 2000, pp. 1656-1662.

[82] T. Zwick, D. Hampicke, J. Maurer, A. Richter, G. Sommerkorn, R. Thomä, and W. Wiesbeck, "Results of double-directional channel sounding measurements," *Proceedings of 51st IEEE Vehicular Technology Conference (VTC 2000-Spring),* Tokyo, Japan, May 15-18, 2000, vol. 3, pp. 2497-2501.

[83] J. Kivinen, P. Suvikunnas, D. Perez, C. Herrero, K. Kalliola, and P.Vainikainen, "Characterization system for MIMO channels," *Proceedings of 4th International Symposium on Wideband Personal Multimedia Communications Conference (WPMC'01),* Aalborg, Denmark, September 9-12, 2001.

[84] C. C. Martin, J. H. Winters, N. R Sollenberger, "Multiple-input multiple-output (MIMO) radio channel measurements," *Proceedings of IEEE 52nd Vehicular Technology Conference (VTC2000-Fall),* Boston, MA, USA, 24-28 September, 2000, vol. 2, pp. 774-779.

[85] D. P. McNamara, M. A. Beach, P. N. Fletcher, and P. Karlsson, "Temporal analysis of indoor multiple-input multiple-output (MIMO) channel measurements," *Proceedings of 4th European Personal Mobile Communications Conference (EPMCC2001)*, Vienna, Austria, February 20-22, 2001, CD-ROM ÖVE 27 (ISBN 3-85133-023-4), pap57.pdf.

[86] J. P. Kermoal, L. Schumacher, P. E. Mogensen, and K. I. Pedersen, "Experimental investigation of correlation properties of MIMO radio channels for indoor picocell scenarios," *Proceedings of IEEE 52nd Vehicular Technology Conference (VTC2000-Fall),* Boston, MA, USA, 24-28 September, 2000, vol. 1, pp. 14-21.

[87] J. Kivinen, *Development of wideband radio channel measurement and modeling techniques for future radio systems,* Doctoral Thesis, Helsinki University of Technology Radio Laboratory Publications, Report S244, 2001,41 p.

[88] K. Kalliola, *Testbed for adaptive array antennas*, Master's Thesis, Helsinki University of Technology, February 1997, 87 p.

[89] J.-P. Rossi, J.-P. Barbot, and A. J. Levy, "Theory and measurement of the angle of arrival and time delay of UHF radiowaves using a ring array," *IEEE Transactions on Antennas and Propagation*, vol. 45, no. 5, pp. 876-884, May 1997.

[90] J. R. Edmundson, "The distribution of point charges on the surface of a sphere," *Acta Crystallographica,* A48, pp. 60-69, 1992.

[91] L. I. Vaskelainen, "Iterative least-squares synthesis methods for conformal array antennas with optimized polarization and frequency properties," *IEEE Transactions on Antennas and Propagation,* vol. 45, no. 7, pp. 1179-1185, July 1997.

[92] J. de Dios, *High-resolution channel parameter estimation for future mobile communication systems*, Master's Thesis, Helsinki University of Technology, 2000, 106 p.

[93] C. Bergljung and L. G. Olsson, "Rigorous diffraction theory applied to street microcell propagation," *Proceedings of the Global Telecommunications Conference 1991 (GLOBECOM '91)*, vol. 2, December 1991, pp. 1292-1296.

[94] Y. S. Yeh, “Antennas and Polarization Effects,” Chapter 3 in *Microwave Mobile Communications Wireless Communication Systems*, editor W. C. Jakes, New York, John Wiley & Sons, 1974, 642 p.

[95] C. A. Balanis, *Antenna Theory, Analysis and Design*, New York, Wiley, 1982, 790 p.

[96] J. Shapira, S. Miller, “A novel polarization smart antenna,” *Proceedings of IEEE 53rd Vehicular Technology Conference (VTC2001 Spring),* Rhodes, Greece, 6-9 May, 2001, vol. 1, pp. 253-257.